THE JOURNAL OF PHYSICAL CHEMISTRY C
A JOURNAL OF THE AMERICAN CHEMICAL SOCIETY

pubs.acs.org/JPCC

Article

NMR Crystallography of Monovalent Cations in Inorganic Matrices: Na^+ Siting and the Local Structure of Na^+ Sites in Ferrierites

Petr Klein, Jiri Dedecek, Haunani M. Thomas, Sarah R. Whittleton, Jiri Klimes, Jiri Brus, Libor Kobera, David L. Bryce, and Stepan Sklenak*

Cite This: J. Phys. Chem. C 2022, 126, 10686−10702

Read Online

ACCESS | Metrics & More | Article Recommendations

ABSTRACT: Zeolites are crystalline microporous aluminosilicates of paramount importance. The siting of cations balancing the negative charge of framework Al affects the catalytic and sorption properties of cation-exchanged zeolites. The siting of Na^+ cations in dehydrated Si-rich ferrierite zeolites is investigated by ^{23}Na (ultra)-high-field (MQ)MAS NMR spectroscopy together with DFT to obtain the Na^+ siting and the local structure of nine Na^+ cationic sites formed by two 6-rings and two 8-rings having one Al atom located in different framework T sites. The occupation of the Na^+ cationic sites is not controlled by their relative energies but by the kinetics of the Na^+ ion-exchange. ^{23}Na solid-state NMR spectroscopy alone can determine the ring forming the Na^+ site but not which T site is occupied by Al in that ring. The developed methodology represents a highly promising tool for the analysis of the Na^+ arrangements in zeolites and other crystalline matrices.

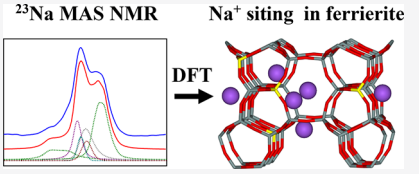

1. INTRODUCTION

Zeolites are the most important group of industrial heterogeneous catalysts.[1] Besides the Y and USY zeolites of the faujasite structure,[2,3] Si-rich zeolites (Si/Al > 8) such as ZSM-5, the beta zeolite, ferrierite, MCM-22, and mordenite show the highest industrial impact.[4,5] Zeolites are crystalline microporous aluminosilicates with 3D channel structures made of corner-sharing TO_4 tetrahedra (T = Si or Al^-). Isomorphous framework Al/Si substitutions result in a negative charge of AlO_4^- tetrahedra, which is balanced by extra-framework cationic species representing active sites for numerous redox- or base-catalyzed reactions.

Cations can be accommodated in extra-framework centers which differ in their coordination, arrangement of the local environment, and location in zeolite channels.[4,5] These characteristics are determined by the siting of the Al atoms of the negatively charged AlO_4^- tetrahedra in the framework crystallographic T sites. Besides protonic forms, transition-metal-exchanged Si-rich zeolites are the most promising since they show unique catalytic redox behavior.[4,5] Several features of Si-rich zeolites strongly limit the applicability of diffraction methods to determine the siting of cations: (i) a high number of crystallographically distinguishable framework T sites of which only some are partly occupied by Al atoms, (ii) a low number of Al atoms in the framework (Si/Al > 8), and (iii) large unit cells.[6,7] Therefore, knowledge regarding the siting of cations and the local structure of cationic sites in Si-rich zeolites is very limited.[4−6,8] However, this information is necessary to gauge the catalytic and sorption properties of cation-exchanged zeolites. Several diffraction studies regarding monovalent cation-exchanged pentasil-ring zeolites have been performed,[8−11] but the cations have been mainly heavy ones (Cs^+ and Tl^+) not very appealing for catalysis.[10,12−16] Diffraction experiments provide only the positions of the cations in the framework but not the local structure of the cationic sites as the coordinates of the cations are combined with the averaged coordinates of the framework, reflecting mainly empty cationic sites and also the corresponding siliceous structures (i.e., without the framework Al/Si substitutions).[6] Conversely, NMR crystallography represents an approach to determine the local structure of cationic centers in Si-rich zeolites. The knowledge of the local structure of active centers is very important in catalysis.

A new approach to determine the Li^+ siting in matrices of Si-rich zeolites was developed in our prior study of Li^+-exchanged ferrierites.[6] This procedure employs high-resolution $^7Li-^7Li$ correlation MAS NMR spectroscopy coupled with periodic DFT calculations of the structure of Li^+ sites and subsequent DFT cluster computations of the ^7Li NMR shielding. Similarly, ^{23}Na solid-state NMR spectroscopy represents a powerful tool to identify the Na^+ siting in matrices of Si-rich zeolites.[17,18] The incorporation of Na^+ cations into diverse matrices has attracted particular attention because of its pivotal importance in various fields such as, for example, energy storage[19] and CO_2 capture.[20−23]

Received: April 11, 2022
Revised: May 30, 2022
Published: June 22, 2022

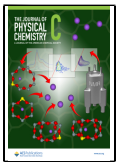

In this paper, we demonstrate a new approach to the determination of the siting of Na^+ and the local structure of Na^+ extra-framework cationic sites in crystalline aluminosilicate matrices based on a combination of high-field and ultra-high-field MAS and MQMAS ^{23}Na NMR spectroscopy interpreted using predictions of the ^{23}Na NMR parameters obtained from periodic DFT calculations including extensive molecular dynamics (MD) simulations. The usage of high-field and ultra-high-field ^{23}Na solid-state NMR permits highly reliable evaluations of the ^{23}Na NMR parameters of Na^+ cations in various cationic sites. While ^{23}Na MAS NMR spectroscopy is used to identify Na^+ cations with a large quadrupolar broadening since the ^{23}Na NMR resonances of such cations are suppressed in ^{23}Na MQMAS NMR experiments, ^{23}Na MQMAS NMR experiments are employed to analyze close overlapping ^{23}Na NMR resonances with a smaller quadrupolar broadening. The results reveal that Na^+ cations can be ligated to oxygen atoms of nine distinct extra-framework cationic sites of which eight are occupied by Na^+ in one or more of the investigated samples. The Na^+ centers are formed by two 6-rings and two 8-rings with one Al atom located in different framework T sites. The occupancy of the cationic sites by Na^+ significantly varies for the studied ferrierites.

This study is the first one which determines the local structure of Na^+ extra-framework cationic sites in a Si-rich zeolite with no knowledge of the Na^+ cationic sites from diffraction experiments. Previously, only Al-rich zeolites with the already known Na^+ cationic sites were studied by ^{23}Na solid-state NMR spectroscopy.[17,18] This investigation is performed on the zeolite of the ferrierite structure, which is an industrially important catalyst.

2. COMPUTATIONAL MODELS AND METHODS

2.1. Structural Models. Five models, possessing the P1 symmetry, featuring one Al/Si substitution in the framework T1a,[24] T1b,[24] T2, T3, and T4 sites[25] and one Na^+ cation compensating for the corresponding negative charge of AlO_4^-, were employed. The models were composed of a super cell consisting of two unit cells (Si/Al 71) along the c dimension. The starting structure of the all-silica zeolite framework (no Na^+) was downloaded from the zeolite structural database.[25] All possible symmetrically non-equivalent Na^+ sites with the Na^+ cations coordinated to two oxygen atoms of the AlO_4^- tetrahedron (with the $Na-O_{Al}$ distances of ca. 2.4 Å) for each of the five models were used as the starting structures.

2.2. Electronic Structure Calculations. The CP2K suite of software[26,27] was employed using the BLYP functional,[28,29] GTH pseudopotentials,[30,31] and the TZV2P-GTH basis set. The energy cutoff of 1120 Ry was used.

2.3. Molecular Dynamics. MD simulations were performed as implemented in the QUICKSTEP program,[26] a part of the CP2K suite of software.[27] Born-Oppenheimer MD simulations of 10,000 fs durations were performed in the canonical ensemble, with a time step of 1.0 fs and a mean temperature of 400 K regulated using a chain of Nose−Hoover thermostats. Similar time lengths were used for MD simulations of cationic sites in zeolites.[32−38] The structures of 20 distinct snapshots collected at 500, 1000, 1500, ... 10,000 fs of the MD simulations were optimized for the five computational models. The most stable structures of all distinct Na^+ sites for all the five models (i.e., Al in all the five framework T sites[24]) were used for subsequent NMR computations.

2.4. Geometry Optimizations. The lattice parameters and the atomic positions were optimized employing conjugate-gradient algorithm minimization of energies and forces as implemented in the QUICKSTEP program,[26] a part of the CP2K suite of software.[27]

2.5. Random Phase Approximation. The calculations employing the random phase approximation (RPA) to the energy were performed using the Vienna ab-initio simulation package (VASP).[39−45] The Perdew−Burke−Ernzerhof functional[46] was used to provide the input states for the RPA calculation. The renormalized singles corrections to the energy[47] (RSE) of Ren and co-workers, as implemented in VASP,[48] were included in the final RPA energy. The calculations were performed using the gamma-point-only k-point sampling. The exact-exchange energy was evaluated using an 800 eV basis-set cut-off, the RSE corrections using a 400 eV basis-set cut-off and the RPA correlation energy using a 500 eV cut-off for orbitals and a 300 eV cut-off for the response function.

2.6. Calculations of ^{23}Na NMR Parameters. Clusters of seven coordination shells around the Al atom ($Al-O-Si-O-Si-O-Si-O-H_{link}$) and the Na^+ cation were extracted from the optimized structures. Due to the presence of silicate rings in the framework of the ferrierite, the created seven-shell clusters contained pairs of very close H_{link} atoms. Since the close H_{link} atoms represented the same Si atom, they were replaced by the corresponding $Si(OH_{link})_2$ moiety. This was repeated until the cluster contained no such pairs. Subsequently, the Gaussian09 program[49] was employed to calculate ^{23}Na NMR shielding tensors, nuclear quadrupolar coupling constants,[50] C_Q, and asymmetry parameters,[50] η, for the ^{23}Na atom by the gauge-independent atomic orbital method[51] using the B3LYP functional[29,52] and the pcS basis sets of Jensen:[53] pcS-4 for the Na and Al atoms and pcS-1 for all the other atoms. The EFGShield program[50] was employed to extract the C_Q and η values from the Gaussian output files. Moreover, the nuclear quadrupolar coupling product P_Q, which is defined[54] as follows: $P_Q = C_Q(1 + \eta^2/3)^{1/2}$, was calculated from the C_Q and η values. These P_Q values can be compared with those obtained from simulations of the measured ^{23}Na MAS NMR and ^{23}Na MQMAS NMR spectra.

2.7. Conversion of the ^{23}Na NMR Shielding Values to ^{23}Na Isotropic Chemical Shifts. The calculated ^{23}Na NMR shielding values were converted to ^{23}Na isotropic chemical shifts using the calculated shielding of 568.6 ppm for $Na^+(H_2O)_6$ (the corresponding ^{23}Na chemical shift is 0.0 ppm by definition).[55] The geometry of $Na^+(H_2O)_6$ was optimized at the B3LYP/cc-pVQZ level, and subsequently, the ^{23}Na NMR shielding of 568.6 ppm was obtained with B3LYP and employing the pcS-4 basis set for the Na atom and the pcS-1 basis set for the O and H atoms. The conversion was further verified employing a secondary standard. A ^{23}Na NMR shielding of 583.1 ppm was calculated for the faujasite structure featuring four Al atoms in the hexagonal prism (i.e., the double 6-rings) and one Na^+ cation accommodated in the SI site employing the experimental structure of Olson[56] using the same procedure as the calculations of ferrierite. The ^{23}Na NMR shielding of 583.1 ppm corresponds to the ^{23}Na NMR resonance of −14 ppm assigned to the SI site in the Na−Y zeolite[18] (Si/Al 2.11) and CsNa−Y zeolite[17] (Si/Al 2.49). The difference between the assignments based on the primary and secondary standards is only 0.5 ppm, confirming a high

https://doi.org/10.1021/acs.jpcc.2c02496
J. Phys. Chem. C 2022, 126, 10686−10702

Table 1. ^{23}Na NMR Parameters (σ, δ_{iso}, C_Q, η, and P_Q) and the Relative Energy of the Na^+ Cationic Sites Calculated for the Computational Models

site	σ (ppm)[a]	δ_{iso} (ppm)[b]	C_Q (MHz)[c]	η[d]	P_Q (MHz)[e]	ΔE (kcal/mol)[f]	ΔE (kcal/mol)[g]
T1-8-ring_1	588.4	−19.8	3.7	0.45	3.8	0.0	0.0
T1-6-ring_1	583.1	−14.5	2.5	0.75	2.7	1.8	1.8
T1-8-ring_2	581.2	−12.6	3.0	0.75	3.3	1.5	1.9
T2-6-ring_2	570.7	−2.1	5.4	0.50	5.7	0.0	0.0
T2-8-ring_1	588.5	−19.9	3.7	0.70	4.0	1.9	3.9
T3-6-ring_1	581.5	−12.9	2.4	0.65	2.6	0.0	0.0
T3-8-ring_2	582.2	−13.6	3.0	0.75	3.3	1.9	3.7
T4-6-ring_2	567.9	0.7	4.9	0.70	5.2	0.0	0.0
T4-8-ring_2	587.1	−18.5	2.7	0.95	3.0	5.9	7.2

[a]^{23}Na NMR shielding. [b]^{23}Na isotropic chemical shift. [c]Nuclear quadrupolar coupling constant. [d]Asymmetry parameter. [e]Nuclear quadrupolar coupling product. [f]Relative energies calculated using the cp2k program. [g]Relative energies calculated using the VASP program employing the RPA approach.

reliability of the conversion of the calculated ^{23}Na NMR shielding values to ^{23}Na isotropic chemical shifts based on the primary standard used in this study.

3. EXPERIMENTAL SECTION

3.1. Sample Preparation. A set of three Na-ferrierite (FER) samples with predominately isolated Al atoms (for definition of isolated Al atoms, see ref 34) in the framework was studied. The three ferrierite samples were the same as those used in our prior studies.[6,24] The parent FER/20 sample with Si/Al of 20 and more than 94%[24] of isolated Al atoms was purchased from Unipetrol, a.s., Czech Republic (FER/A in ref 24). The FER/27 sample (Si/Al 27, more than 96%[24] of isolated Al, FER/B in ref 24) was synthesized using pure silica (Cab−O−Sil M5), sodium and aluminum sulfate, NaOH, and pyridine as the structure directing agent. The FER/30 sample (Si/Al 30, more than 96%[24] of isolated Al, FER/C in ref 24) was purchased from Zeolyst International, Inc. Details regarding the sample preparations and characterization of the corresponding Al organizations (for definition of the Al organization, see ref 34) are described elsewhere.[24]

The parent NaK-samples of FER/20 and FER/27 were ion-exchanged with 0.5 M NH_4NO_3 twice for 24 h to obtain NH_4 forms. The NH_4-FER/20 and NH_4-FER/27 together with the parent NH_4-FER/30 were further equilibrated into Na-FER forms by repeated (3 × 24 h) Na^+ ion-exchange using a 0.5 M solution of $NaNO_3$ (50 mL per 1 g of a zeolite) at room temperature. Subsequently, the samples were filtered and thoroughly washed with distilled water.

For the analysis of the siting of Na^+ in extra-framework cationic positions, the three Na-FER samples were dehydrated to enable the coordination of bare Na^+ cations to the zeolite framework and the occupation of the cationic sites. Prior to the dehydration, the hydrated samples were packed into ZrO_2 MAS NMR rotors and dried overnight in an oven at 100 °C to remove excess water. The dehydrated Na-FER samples for the NMR experiments were prepared "in situ" using an instrumental setup that allows dehydration and subsequent sealing of the cooled Na-FER samples in NMR rotors under vacuum. The samples were dehydrated at 450 °C under dynamic vacuum of $p = 1 \times 10^{-1}$ Pa for 3 h with a heating ramp of 3 °C min^{-1}. Subsequently, the Na-FER samples were cooled down to room temperature and airtight-sealed with Kel-F cups. The sealed rotors were immediately transferred into glass tubes, which were evacuated and sealed to prevent rehydration of the samples before NMR experiments.

3.2. Solid-State NMR Experiments at 500 MHz. Experiments were carried out using a Bruker AVANCE III HD 500 WB/US three-channel NMR spectrometer equipped with a wide-bore ultra-stabilized magnet charged to 11.7 T ($\nu_0(^1H)$ = 500 MHz). ^{23}Na MAS NMR spectra were acquired at a Larmor frequency, $\nu_0(^{23}Na)$, of 132.3 MHz using either a 4 mm double-resonance MAS probe or a 3.2 mm double-resonance MAS probe at spinning frequencies of ν_{rot} = 12 kHz and ν_{rot} = 20 kHz, respectively. The one-dimensional ^{23}Na MAS NMR single-pulse spectra were collected using single-pulse excitation and high-power proton decoupling. An optimized pulse width ranging from 2.3 to 4.4 μs and a recycle delay of 4 s were used with the number of scans ranging from 2560 to 3072 and the spectral widths ranging from 40 to 55 kHz. The two-dimensional ^{23}Na MQMAS NMR spectra were recorded using the three-pulse z-filtered sequence[57] with selective, excitation, and conversion pulse widths of 6.8, 2.1, and 35 μs for the 4 mm probe, respectively, and 5.0, 2.0, and 18 μs for the 3.2 mm probe, respectively. The number of increments in the indirect dimension was set to 256, each made with 1024−2048 scans.

3.3. Solid-State NMR Experiments at 900 MHz. Experiments were performed using a Bruker AVANCE II 4-channel NMR spectrometer equipped with a narrow-bore ultra-stabilized 21.1 T ($\nu_0(^1H)$ = 900.08 MHz) magnet. ^{23}Na MAS NMR spectra were measured at a Larmor frequency, $\nu_0(^{23}Na)$, of 238.1 MHz using a 4 mm double-resonance MAS probe. The dehydrated samples were spun in 4 mm o.d. ZrO_2 rotors at a spinning frequency of ν_{rot} = 10 kHz. The one-dimensional ^{23}Na MAS NMR single-pulse spectra were collected with 2048 scans using a single-pulse excitation with an optimized pulse width of 1 μs and relaxation delay of 1 s. The two-dimensional ^{23}Na MQMAS NMR spectra were recorded using the three-pulse z-filtered sequence with selective, excitation, and conversion pulse widths of 5.2, 2.1, and 20 μs, respectively. The number of increments in the indirect dimension was 512, each made with 576 scans.

The ^{23}Na chemical shifts were referenced externally to a 1 M solution of NaCl (δ_{iso} = 0.0 ppm) using a secondary reference of solid NaCl at 7.2 ppm. The fitting of the one-dimensional single-pulse and two-dimensional ^{23}Na MQMAS NMR spectra were performed using the DmFit software.[58]

4. COMPUTATIONAL RESULTS

4.1. Calculation of the Cationic Sites and the NMR Parameters. Our calculations of the models of the Na^+

https://doi.org/10.1021/acs.jpcc.2c02496
J. Phys. Chem. C 2022, 126, 10686−10702

cationic sites yielded three, two, two, and two Na^+ cationic sites (Table 1) for Al(T1), Al(T2), Al(T3), and Al(T4), respectively. The Na^+ sites for Al(T1a)[24] and Al(T1b)[24] are the same. The coalescence of the cationic sites for Al(T1a)[24] and Al(T1b)[24] was calculated for Li^+ as well.[6] Subsequent NMR calculations gave the corresponding ^{23}Na NMR parameters (Table 1).

The Na^+ cationic sites can be naturally sorted according to the rings forming these sites rather than by the crystallographically distinguishable framework T sites occupied by the Al atom (i.e., the Al siting[34]). The cationic sites formed by the same ring with different Al sitings have similar NMR parameters. The optimized structures, ^{23}Na isotropic chemical shift (δ_{iso}), nuclear quadrupolar coupling constant (C_Q), and asymmetry parameter (η) are shown in Figures 1–4.

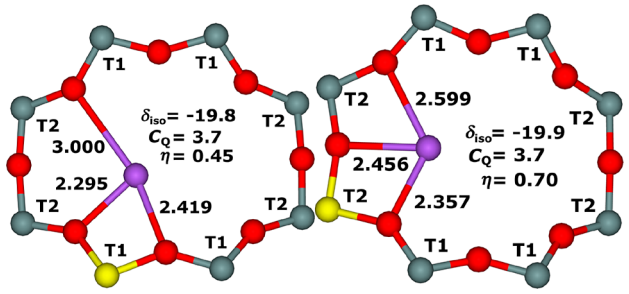

Figure 1. Optimized structure (Na–O distances in Å) of the Na^+ cationic sites with the designations of the T sites for the T2-T2-T1-T1-T2-T2-T1-T1 8-rings (i.e., 8-ring_1), the ^{23}Na isotropic chemical shift (δ_{iso}) in ppm, the nuclear quadrupolar coupling constant (C_Q) in MHz, and the asymmetry parameter (η); the T1-8-ring_1 cationic site (left) and the T2-8-ring_1 cationic site (right). Silicon atoms are in gray, oxygen atoms in red, aluminum atoms in yellow, and sodium in violet.

The side views of the Na^+ centers showing planarity/non planarity of the cationic sites are depicted in Figure 5.

4.2. Na^+ Cationic Sites Formed by the T2-T2-T1-T1-T2-T2-T1-T1 8-Ring (i.e., 8-Ring_1). Figure 1 shows that the T2-T2-T1-T1-T2-T2-T1-T1 8-rings, hereafter 8-ring_1, forms Na^+ cationic sites for both possible Al sitings [i.e., Al(T1) and Al(T2)]. The Na^+ cation is coordinated to two O atoms of the AlO_4^- tetrahedron (Na–O_{Al} distances of 2.30 and 2.42 Å for T1-8-ring_1 and 2.36 and 2.46 Å for T2-8-ring_1) and to one O atom of one SiO_4 tetrahedron (Na–O_{Si} distance of 3.00 Å for T1-8-ring_1 and 2.60 Å for T2-8-ring_1). The Na^+ is positioned slightly above the plane of the oxygen atoms to which it is coordinated for both the sites (Figure 5). The

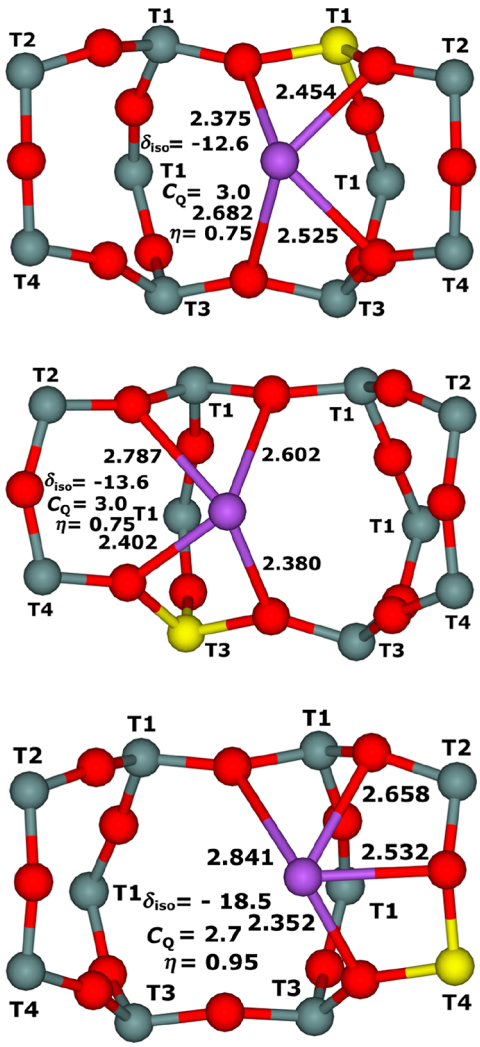

Figure 3. Optimized structure (Na–O distances in Å) of the Na^+ cationic sites with the designations of the T sites for the T4-T2-T1-T1-T2-T4-T3-T3 8-rings (i.e., 8-ring_2), the ^{23}Na isotropic chemical shift (δ_{iso}) in ppm, the nuclear quadrupolar coupling constant (C_Q) in MHz, and the asymmetry parameter (η); the T1-8-ring_2 cationic site (top), the T3-8-ring_2 cationic site (middle), and the T4-8-ring_2 cationic site (bottom). Silicon atoms are in gray, oxygen atoms in red, aluminum atoms in yellow, and sodium in violet.

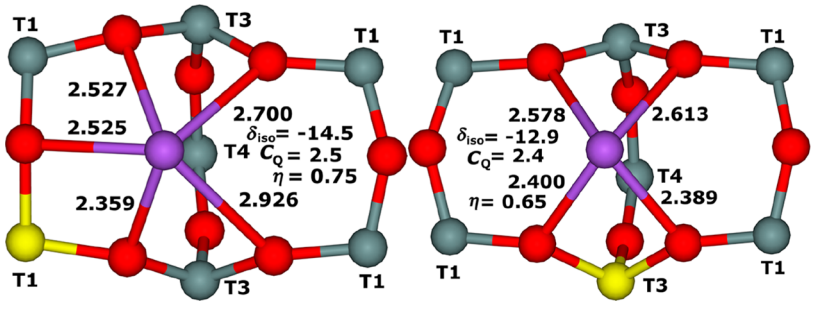

Figure 2. Optimized structure (Na–O distances in Å) of the Na^+ cationic sites with the designations of the T sites for the T1-T1-T3-T1-T1-T3 6-rings (i.e., 6-ring_1), the ^{23}Na isotropic chemical shift (δ_{iso}) in ppm, the nuclear quadrupolar coupling constant (C_Q) in MHz, and the asymmetry parameter (η); the T1-6-ring_1 cationic site (left) and the T3-6-ring_1 cationic site (right). Silicon atoms are in gray, oxygen atoms in red, aluminum atoms in yellow, and sodium in violet.

https://doi.org/10.1021/acs.jpcc.2c02496
J. Phys. Chem. C 2022, 126, 10686–10702

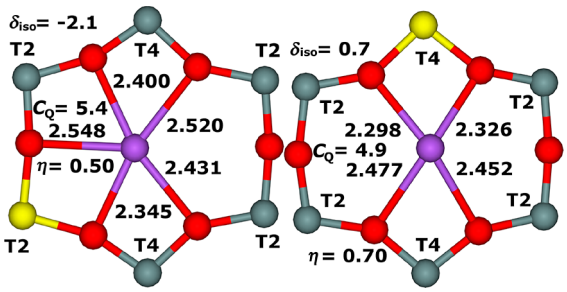

Figure 4. Optimized structure (Na−O distances in Å) of the Na^+ cationic sites with the designations of the T sites for the T2-T2-T4-T2-T2-T4 6-rings (i.e., 6-ring_2), the ^{23}Na isotropic chemical shift (δ_{iso}) in ppm, the nuclear quadrupolar coupling constant (C_Q) in MHz, and the asymmetry parameter (η); the T2-6-ring_2 cationic site (left) and the T4-6-ring_2 cationic site (right). Silicon atoms are in gray, oxygen atoms in red, aluminum atoms in yellow, and sodium in violet.

calculated values of the ^{23}Na isotropic chemical shift (δ_{iso}) and the nuclear quadrupolar coupling constant (C_Q) are very close for both the sites (δ_{iso} = −20 ppm and C_Q = 3.7 MHz, respectively). Conversely, the asymmetry parameter (η) significantly differs: 0.45 and 0.70 for the T1-8-ring_1 and T2-8-ring_1, respectively.

4.3. Na^+ Cationic Sites Formed by the T1-T1-T3-T1-T1-T3 6-Ring (i.e., 6-Ring_1). Figure 2 shows that the T1-T1-T3-T1-T1-T3 6-rings, hereafter 6-ring_1, creates Na^+ cationic sites for both possible Al sitings (i.e., Al(T1) and Al(T3)). The Na^+ cation is ligated to two O atoms of the AlO_4^- tetrahedron (Na−O_{Al} distances of 2.36 and 2.53 Å for T1-6-ring_1 and 2.39 and 2.40 Å for T3-6-ring_1) and to three O atoms of two SiO_4 tetrahedra for T1-6-ring_1 (Na−O_{Si} distances of 2.53, 2.70, and 2.93 Å) or to two O atoms of one SiO_4 tetrahedron for T3-6-ring_1 (Na−O_{Si} distances of 2.58 and 2.61 Å). Na^+ is positioned markedly above the plane of the oxygen atoms to which it is ligated for both the sites (Figure 5). Our calculations yielded similar ^{23}Na isotropic chemical shifts of −13 to −15 ppm, a nuclear quadrupolar coupling constant of ca. 2.5 MHz, and an asymmetry parameter of ca. 0.7 for both the sites.

4.4. Na^+ Cationic Sites Formed by the T4-T2-T1-T1-T2-T4-T3-T3 8-Rings (i.e., 8-Ring_2). There are four possible Al sitings in the T4-T2-T1-T1-T2-T4-T3-T3 8-rings, hereafter 8-ring_2, making Na^+ cationic sites. Figure 3 shows the calculated sites for Al(T1), Al(T3), and Al(T4). Conversely, our calculations yielded no Na^+ cationic site for Al(T2). The Na^+ cation binds to two O atoms of the AlO_4^- tetrahedron and two O atoms of one SiO_4 tetrahedron for all the three Al sitings. The Na−O_{Al} distances are calculated to lie in the range from 2.35 to 2.53 Å, while the Na−O_{Si} distances are longer, ranging from 2.53 to 2.84 Å. Na^+ is located significantly above the plane of the oxygen atoms forming the cationic center for all the three sites (Figure 5). The calculated ^{23}Na isotropic chemical shifts (δ_{iso} = ca. −13 ppm), the nuclear quadrupolar coupling constant (C_Q = 3.0 MHz), and the asymmetry parameter (η = 0.75) are very close for T1-8-ring_2 and T3-8-ring_2, while these values differ (more negative δ_{iso} of −19 ppm, smaller C_Q of 2.7 MHz, and larger η of 0.95) for T4-8-ring_2.

4.5. Na^+ Cationic Sites Formed by the T2-T2-T4-T2-T2-T4 6-Rings (i.e., 6-Ring_2). Figure 4 shows two cationic sites created by the T2-T2-T4-T2-T2-T4 6-rings, hereafter 6-ring_2, for both the possible Al sitings. The Na^+ cation is tightly coordinated to five and four O atoms for Al(T2) and Al(T4) sitings, respectively, and lies in the plane and slightly above the plane, respectively, of the 6-ring_2 (Figure 5). The Na−O_{Al} distances are calculated to be 2.35 and 2.55 Å for Al(T2) and 2.30 and 2.33 Å for Al(T4), while the Na−O_{Si} distances are somewhat longer [2.40, 2.43, and 2.52 Å for Al(T2) and 2.45 and 2.48 Å for Al(T4)]. The calculated NMR parameters differ for both the sites. The δ_{iso} of −2 ppm for T2-6-ring_2 is more negative than the δ_{iso} of 1 ppm for T4-6-ring_2. The C_Q of 5.4 MHz for T2-6-ring_2 is larger than the C_Q of 4.9 MHz for T4-6-ring_2. The η of 0.50 for T2-6-ring_2 is smaller than the η of 0.70 for T4-6-ring_2.

4.6. Stability of the Cationic Sites. Table 1 also lists the relative energies for the Na^+ cationic sites corresponding to the same Al siting. For a particular Al siting, the sites with the relative energies smaller than ca. 2.0 kcal/mol with respect to the most stable Na^+ cationic site exist in the sample at room temperature.[6] However, this is true only if all the Na^+ cationic sites are accessible during the Na^+ exchange, that is, if the occupation of the Na^+ cationic sites during the Na^+ exchange is driven by thermodynamics.[6] Conversely, if the barrier for Na^+ to occupy a particular cationic site during the Na^+ exchange is

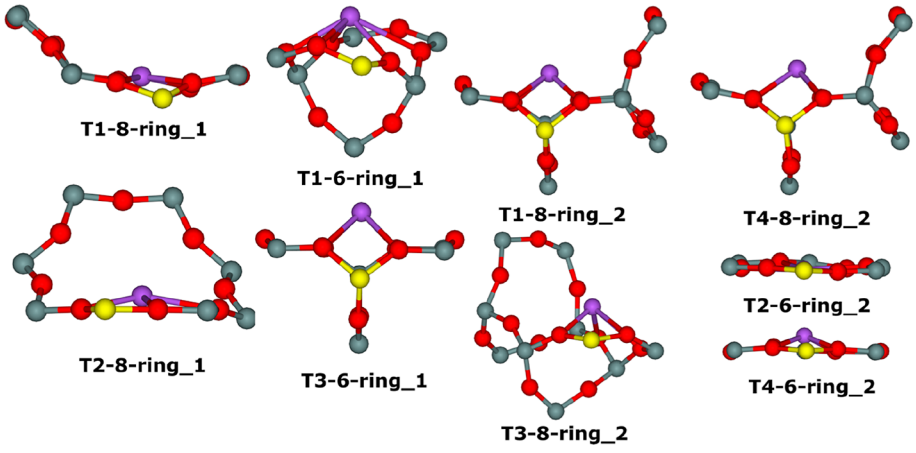

Figure 5. Side views of the optimized structure of the Na^+ cationic sites. Silicon atoms are in gray, oxygen atoms in red, aluminum atoms in yellow, and sodium in violet.

https://doi.org/10.1021/acs.jpcc.2c02496
J. Phys. Chem. C 2022, 126, 10686−10702

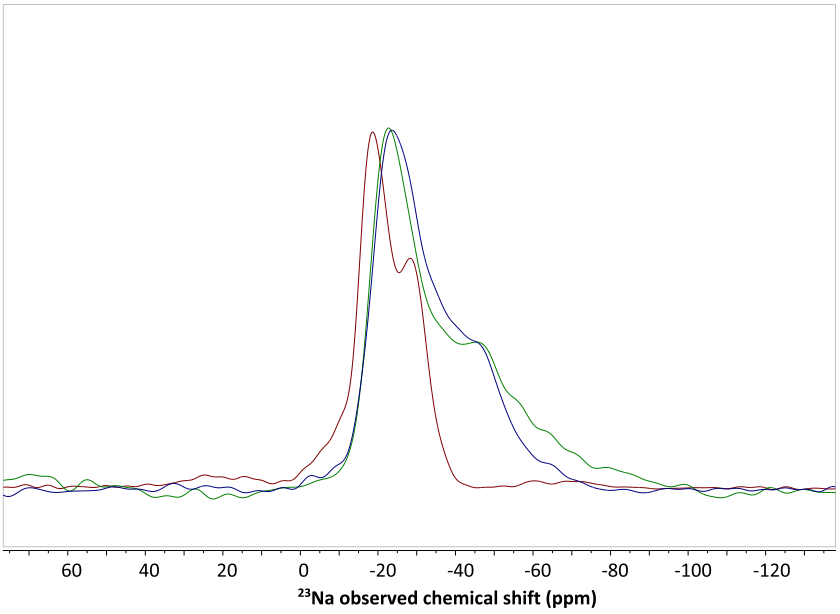

Figure 6. ^{23}Na MAS NMR spectra of Na-FER/20 recorded (i) at B_0 = 21.1 T and ν_{rot} = 10 kHz (brown), and (ii) at B_0 = 11.7 T and ν_{rot} = 12 kHz (blue) and ν_{rot} = 20 kHz (green).

high, then other less thermodynamically favored sites can be occupied.

5. EXPERIMENTAL RESULTS

5.1. ^{23}Na NMR Results. The effect of the spinning frequency and the field strength (B_0) on the ^{23}Na MAS NMR spectrum of the dehydrated Na-ferrierite is shown in Figure 6 showing the spectra of Na-FER/20 recorded at B_0 = 21.1 T with the spinning frequency of 10 kHz and at B_0 = 11.7 T with the spinning frequencies of 12 kHz and 20 kHz.

The spectra recorded at 11.7 T are very broad (about 70 ppm). This agrees with the well-known quadrupolar character of ^{23}Na nuclei[59,60] and the nuclear quadrupolar coupling constant (C_Q) and the asymmetry parameter (η) of the electric field gradient (EFG) tensor of $^{23}Na^+$ accommodated in the cationic sites in the dehydrated ferrierite (Table 1). The narrowing effect of a faster rotation on the spectrum recorded at B_0 = 11.7 T with the spinning frequency of 20 kHz results from the averaging of the first-order quadrupolar interaction, which is rotation-dependent. However, the effect of the spinning frequency on the spectrum of Na-FER/20 is small and does not remove the second-order quadrupolar broadening to allow a detailed analysis of the spectra as the individual resonances of quadrupolar nuclei can take on various shapes depending on the nuclear quadrupolar coupling constant (C_Q) and the asymmetry parameter (η) of the EFG tensor; for details regarding spectral shapes, see ref 59. The significant decrease of the breadth of the spectrum recorded at B_0 = 21.1 T by a factor of 2 relative to that measured at B_0 = 11.7 T is caused by a suppression of the quadrupolar interaction by the higher magnetic field. However, although a significant narrowing of the spectrum was reached at B_0 = 21.1 T, the high values of C_Q and η predicted for $^{23}Na^+$ located in the cationic sites (Table 1) can lead to well-known non-Gaussian shapes of the individual resonances even in this ultra-high field. Therefore, MQMAS experiments were performed to obtain the quadrupolar parameters of the individual ^{23}Na NMR resonances to permit an interpretation of the ^{23}Na MAS NMR spectra.

The ^{23}Na MAS NMR spectra and isotropically sheared 2D projections of ^{23}Na MQMAS NMR spectra of the dehydrated samples Na-FER/20, Na-FER/27, and Na-FER/30 recorded at B_0 = 11.7 T with ν_{rot} = 12 kHz and B_0 = 21.1 T with ν_{rot} = 10 kHz are shown in Figures 7−9. Note that different shapes of the 2D projections of the ^{23}Na MQMAS NMR spectra as well as a substantial decrease of the breadth of the MAS dimension (F_2, horizontal) of the 2D projections of the same sample recorded at different magnetic fields result from the suppression of the quadrupolar interaction at the ultra-high field. Furthermore, rotational sidebands are observed in the ^{23}Na MQMAS NMR spectra recorded at 21.1 T. The experiment at the ultra-high field is also associated with a significantly higher signal to noise ratio partly due to the significant decrease of the breadth of the spectra. A detailed visual inspection of the 2D projections of the ^{23}Na MQMAS NMR spectra indicates the presence of several resonances in each spectrum. However, all the resonances found in the ^{23}Na MQMAS spectra correspond to the main peaks in the ^{23}Na MAS NMR spectra. Conversely, the resonances observed at above (i.e., less negative or even positive) −10 ppm (R−I, see below) at B_0 = 21.1 T are observable only in the ^{23}Na MAS NMR spectra at both the field strengths. This is most likely due to a lower sensitivity of MQMAS to sites with larger quadrupolar coupling constants. Concluding, both the ^{23}Na MAS NMR and ^{23}Na MQMAS NMR spectra of all three dehydrated samples are complex, and a simple visual inspection of the spectra does not allow for their analysis and interpretation. Therefore, we extracted the NMR parameters of the individual resonances from the spectra based on the simultaneous fitting of both the ^{23}Na MAS NMR and ^{23}Na MQMAS NMR spectra. This approach minimizes the bias, which can occur due to overlapping resonances when the traditional approach for the spectra interpretation based on a fitting of cross-sectional traces in the center of gravity of the individual resonances is used. The ^{23}Na MAS NMR and ^{23}Na

https://doi.org/10.1021/acs.jpcc.2c02496
J. Phys. Chem. C 2022, 126, 10686−10702

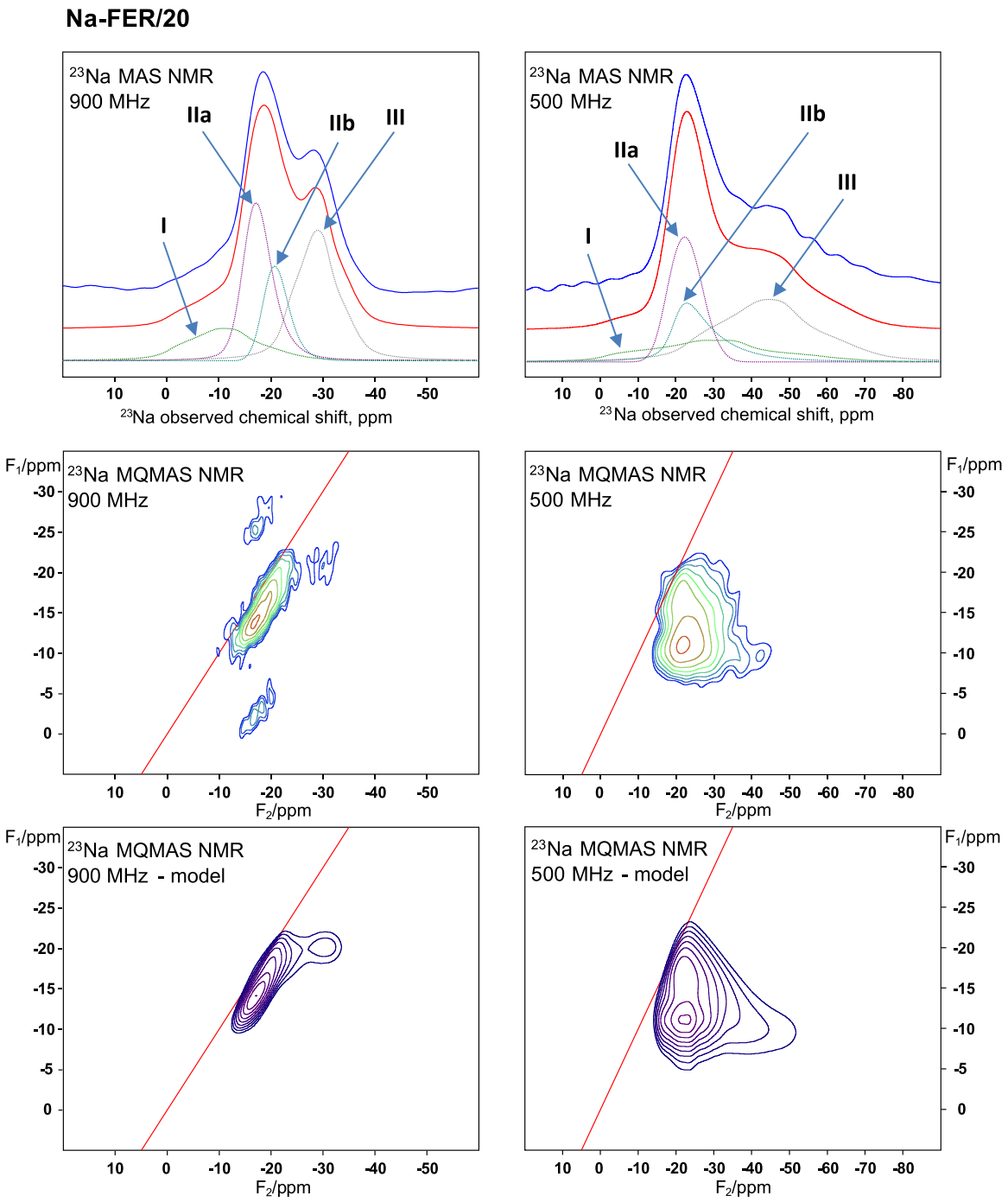

Figure 7. Experimental (solid blue line) and modeled [simulations of the individual sodium sites (dashed lines) and their sum (solid red line)] ^{23}Na MAS and MQMAS NMR spectra of the Na-FER/20 sample recorded at B_0 = 21.1 T (900 MHz) and B_0 = 11.7 T (500 MHz).

MQMAS NMR spectra acquired at two different field strengths (i.e., four spectra for each sample) were simultaneously fitted using the DmFit software[58] to obtain and verify the NMR parameters of the individual ^{23}Na NMR resonances in each sample. Since the NMR parameters reflect the structure and environment around the nuclei in the sample (it should be noted that the structure and environment are properties of the measured material and they are not field-dependent), all the experimental line shapes were fitted using a set of resonances with unique three parameters (δ_{iso}, C_Q, and η) of the same or very similar values for all the four spectra. The spectral simulations are also shown in Figures 7−9. The NMR parameters of the individual resonances obtained are presented in Table 2. Four resonances were identified in the Na-FER/20 and Na-FER/27 samples, while six resonances were found for the Na-FER/30 sample. The relative intensities of the individual resonances (Table 2) were calculated only from the simulations of the ^{23}Na MAS NMR spectra since the MQMAS experiments are not quantitative.

6. DISCUSSION

6.1. Accommodation of Na^+ in Cationic Sites in Ferrierite. Table 1 shows that the DFT-calculated values of (i) the ^{23}Na isotropic chemical shift (δ_{iso}), (ii) the nuclear

https://doi.org/10.1021/acs.jpcc.2c02496
J. Phys. Chem. C 2022, 126, 10686−10702

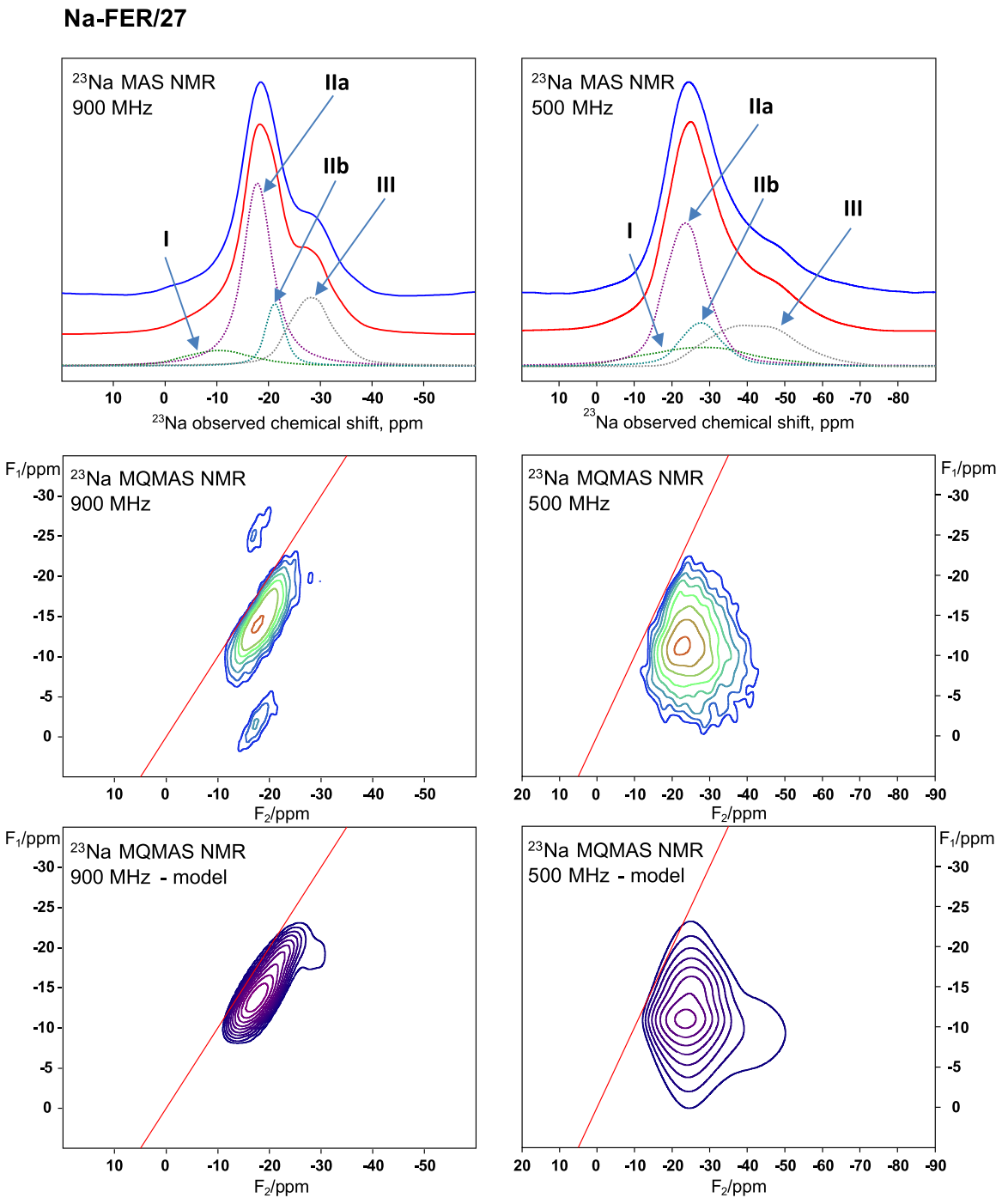

Figure 8. Experimental (solid blue line) and modeled [simulations of the individual sodium sites (dashed lines) and their sum (solid red line)] ^{23}Na MAS and MQMAS NMR spectra of the Na-FER/27 sample recorded at B_0 = 21.1 T (900 MHz) and B_0 = 11.7 T (500 MHz).

quadrupolar coupling constant (C_Q), and (iii) the asymmetry parameter (η) lying in the intervals from 0.7 to −19.9 ppm, from 2.4 to 5.4 MHz, and from 0.45−0.95, respectively, are in very good agreement with the experimental ones (Table 2) ranging from 1.0 to −23.0 ppm, 1.1 to 4.5 MHz, and 0.6 to 0.7, respectively. In addition, the patterns of the predicted and observed ^{23}Na isotropic chemical shifts and the nuclear quadrupolar coupling constants show notable similarities. This confirms the reliability of the calculated Na^+ structures in the ferrierite matrix and the corresponding predicted NMR parameters. The arrangements and properties of Na^+ in the cationic sites in ferrierite and the relation between the coordination of Na^+ cations in the individual sites and the related NMR parameters are discussed based on the calculated NMR parameters to minimize a possible bias due to the experimental errors (e.g., a possibility of a small fraction of Na^+ structures related to Al pairs present in the zeolite samples).

There is only one available experimental structure of a monovalent cation-exchanged dehydrated ferrierite to the best of our knowledge discussed later.[9] Except for this K-ferrierite structure, there are only available experimental data regarding the siting of divalent cations in the dehydrated ferrierite zeolite.[62−64] However, the siting of divalent cations is influenced by the need for the presence of two Al atoms in

https://doi.org/10.1021/acs.jpcc.2c02496
J. Phys. Chem. C 2022, 126, 10686−10702

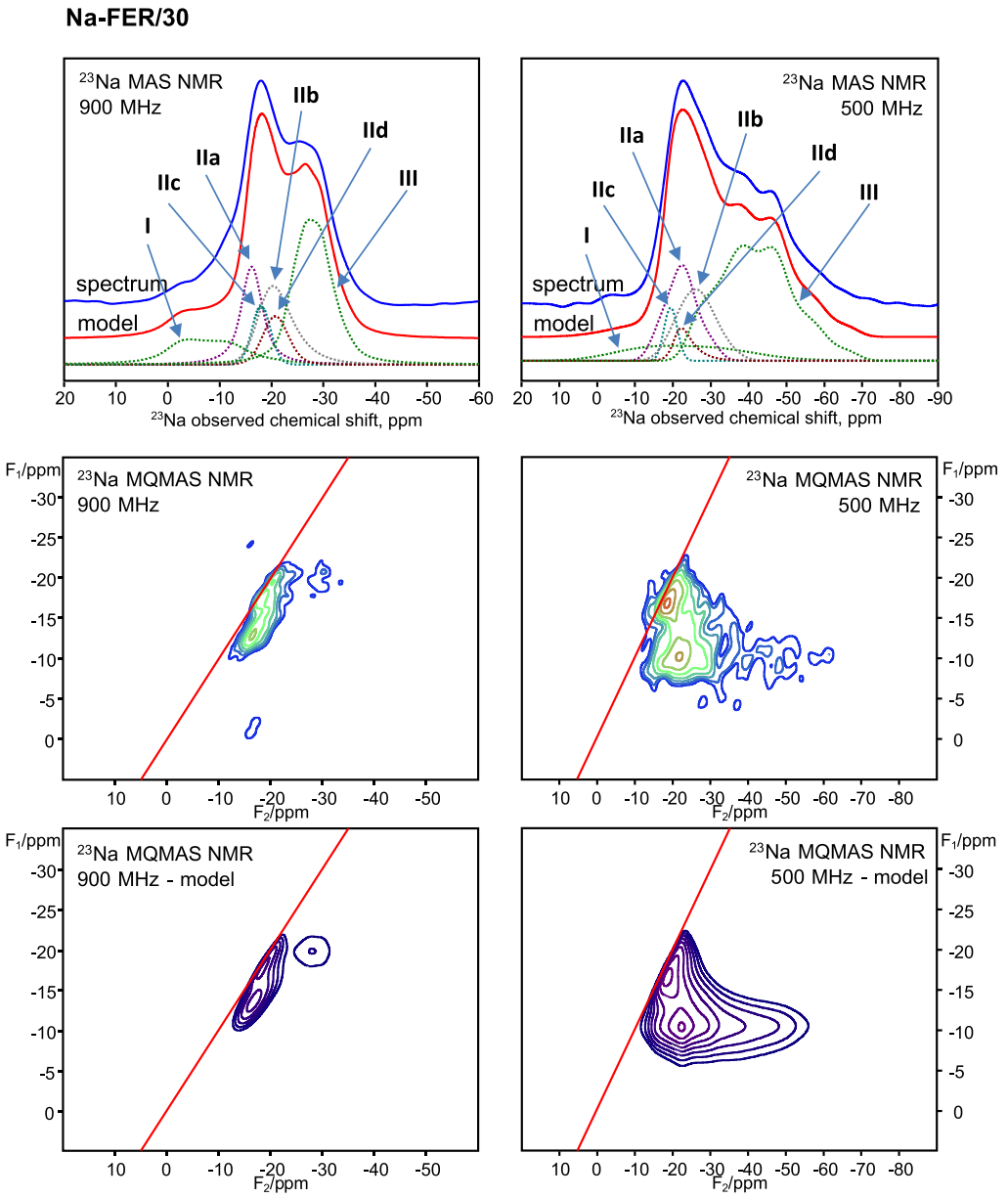

Figure 9. Experimental (solid blue line) and modeled [simulations of the individual sodium sites (dashed lines) and their sum (solid red line)] ^{23}Na MAS and MQMAS NMR spectra of the Na-FER/30 sample recorded at B_0 = 21.1 T (900 MHz) and B_0 = 11.7 T (500 MHz).

the ring forming the corresponding cationic site for bare divalent cations. In contrast to Al-rich zeolites, the fulfilment of this requirement is not guaranteed for all rings of Si-rich zeolite frameworks. Moreover, transition-metal cations, for example, Co^{2+} and Ni^{2+}, are of a significantly smaller diameter compared to the monovalent Na^+ cation. Therefore, large differences between the siting of a monovalent Na^+ cation and that of divalent transition-metal cations are expected.

Visual inspection of the ferrierite framework topology permits the evaluation and comparison of the calculated cationic sites. The cationic site formed by 6-ring_1 (Figure 2) corresponds to the B site according to Mortier's notation.[8] Moreover, if two Al atoms are present in 6-ring_1, then this corresponds to the α site.[24] This site is located on the wall of the main channel and thus accessible through the 10-rings. 6-ring_2 (Figure 4) relates to the A site of Mortier's notation[8] and β site of divalent cations if two Al atoms are present.[24] This site in the ferrierite side channel is accessible through 8-ring_1 (Figure 1). The corresponding cation site formed by 8-ring_1 is equal to the F site of Mortier's notation.[8] 8-ring_1 represents an opening of the ferrierite side channel from the main one, and thus the corresponding site is accessible through the 10-rings. The site created by 8-ring_2 (Figure 3) is located on the wall of the side channel, and it has not been suggested yet. This cationic site is accessible through 8-ring_1. The "boat-shaped" γ site[65] for divalent cations in the side channel is not occupied by Na^+; however, 8-ring_2 represents a part of this complex site. Figure 5 shows that all the calculated Na^+ sites exhibit an open coordination sphere. This feature in combination with the accessibility of the Na^+ sites by 8-rings or 10-rings makes them possible active sites.

6.2. ^{23}Na NMR Parameters and the Local Arrangements of Na^+ in the Cationic Sites. The relationship between the calculated ^{23}Na isotropic chemical shifts (δ_{iso}) and the calculated nuclear quadrupolar coupling constant (C_Q) of Na^+ cations (Table 1) is shown in Figure 10.

https://doi.org/10.1021/acs.jpcc.2c02496
J. Phys. Chem. C 2022, 126, 10686−10702

Table 2. ^{23}Na NMR Parameters (δ_{iso}, C_Q, η, and P_Q) and Relative Intensity (I) of the Individual Na^+ Resonances of the Na-FER Samples

sample	res.	δ_{iso}/ppm[a]	C_Q/MHz[b]	η[c]	P_Q/MHz[d]	I/%	Na^+ site
Na-FER/20	I	0.0 ± 2.0	4.5 ± 0.3	0.7 ± 0.3	4.9 ± 0.3	16	T4-6-ring_2
	IIa	−15.3 ± 1.0	2.1 ± 0.1	0.6 ± 0.1	2.2 ± 0.1	29	T3-8-ring_2
	IIb	−19.2 ± 2.0	2.0 ± 0.2	[e]	2.2 ± 0.2	16	T4-8-ring_2
	III	−23.0 ± 2.0	3.6 ± 0.1	0.7 ± 0.1	3.9 ± 0.1	40	T2-8-ring_1
Na-FER/27	I	−1.5 ± 2.0	4.3 ± 0.3	0.6 ± 0.3	4.6 ± 0.3	12	T4-6-ring_2
	IIa	−15.5 ± 1.0	2.2 ± 0.1	0.6 ± 0.1	2.3 ± 0.1	50	T3-8-ring_2
	IIb	−19.5 ± 2.0	2.1 ± 0.2	0.6 ± 0.1	2.2 ± 0.2	12	T4-8-ring_2
	III	−22.0 ± 2.0	3.6 ± 0.1	0.6 ± 0.1	3.8 ± 0.1	26	T2-8-ring_1
Na-FER/30	I	1.0 ± 2.0	4.4 ± 0.3	[e]	4.7 ± 0.3	12	T4-6-ring_2
	IIa	−14.3 ± 1.0	2.1 ± 0.1	0.7 ± 0.2	2.3 ± 0.1	16	T1-8-ring_2
	IIb	−17.6 ± 2.0	2.3 ± 0.2	0.6 ± 0.2	2.4 ± 0.2	17	T4-8-ring_2
	IIc	−17.5 ± 0.5	1.1 ± 0.1	0.6 ± 0.1	1.2 ± 0.1	6	T3-6-ring_1
	IId	−20.2 ± 0.5	1.3 ± 0.1	[e]	1.4 ± 0.2	6	T1-6-ring_1
	III	−22.8 ± 0.5	3.4 ± 0.1	0.6 ± 0.1	3.6 ± 0.1	44	T1-8-ring_1

[a] ^{23}Na isotropic chemical shift. [b] Nuclear quadrupolar coupling constant. [c] Asymmetry parameter. [d] Nuclear quadrupolar coupling product. [e] This resonance was fitted using a Czjzek function,[61] since the η exhibits a Gaussian distribution.

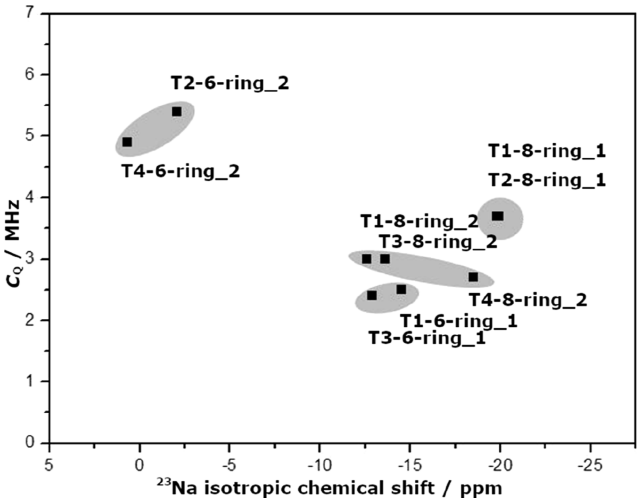

Figure 10. DFT-computed nuclear quadrupolar coupling constants (C_Q) compared to the DFT-computed ^{23}Na isotropic chemical shifts for the nine calculated Na^+ cationic sites.

Figure 2 shows that the Al siting in the T1 and T3 sites has only a small effect on the NMR (i.e., δ_{iso}, C_Q, and η) parameters of Na^+ accommodated in 6-ring_1. Regarding 8-ring_1 (Figure 1) with Al(T1) and Al(T2), δ_{iso} and C_Q are identical while η differs. Concerning 8-ring_2 (Figure 3), the NMR parameters are very close for Al(T1) and Al(T3), while they significantly differ for Al(T4). Conversely, the two Na^+ sites formed by 6-ring_2 are distinguishable from each other since they have distinct NMR parameters (Figure 4). Figure 10 clearly shows that both δ_{iso} and C_Q are significantly more sensitive to the type of ring forming the corresponding cationic site than to the Al siting in the ring. ^{23}Na solid-state NMR spectroscopy thus can provide, without any doubt, the information on the ring accommodating the Na^+ cation, while the Al siting in the ring can be distinguished only for some specific cases [i.e., Al(T4)].

Although, in general, the NMR parameters (i.e., δ_{iso}, C_Q, and η) cannot be predicted empirically and quantum chemical calculations are required, we make an attempt to draw some rough conclusions on the relationship between the arrangement of the cationic sites and the corresponding NMR parameters. Table 1 and Figures 1−5 show that the calculated nuclear quadrupolar coupling constant (C_Q) is the largest for the planar or near-planar sites (T2-6-ring_2 and T4-6-ring_2, respectively, having C_Q = 5.4 and 4.9 MHz, respectively), while C_Q is the smallest (from 2.4 to 3.0 MHz) for the sites with the Na^+ cation positioned markedly above the plane of the oxygen atoms to which it is ligated (i.e., T1-6-ring_1, T3-6-ring_1, T1-8-ring_2, T3-8-ring_2, and T4-8-ring_2). Therefore, it is apparent that C_Q reflects approximate local site symmetry.

The cationic sites which are highly asymmetric but possess an approximately planar Na^+ coordination, that is, T1-8-ring_1 and T2-8-ring_1, have the most negative (ca. −20 ppm) ^{23}Na isotropic chemical shift and a C_Q of 3.7 MHz. The (near) planar sites with a high symmetry, that is, T2-6-ring_2 and T4-6-ring_2, exhibit the least negative or even positive (ca. 0 ppm) ^{23}Na isotropic chemical shift and the highest C_Q of ca. 5 MHz. The sites with the Na^+ cation positioned markedly above the plane of the oxygen atoms to which it is ligated, that is, T1-6-ring_1, T3-6-ring_1, T1-8-ring_2, T3-8-ring_2, and T4-8-ring_2, feature a ^{23}Na isotropic chemical shift from −13 to −15 ppm (T4-8-ring_2 is the exception due to a highly asymmetric coordination of the Na^+ with the δ_{iso} of −19 ppm) and a C_Q from 2.4 to 3.0 MHz.

All the cationic sites except for the T4-8-ring_2 site, which is an outlier, can be sorted into three groups according to the similarity regarding the NMR parameters as well as the closeness of the structures. The latter can be explained by the fact that the Na^+ cation is bound to the oxygen atoms of the cationic sites and optimizes the number and arrangement of the oxygen ligands to reach an energetically favorable position. The T1-8-ring_1 and T2-8-ring_1 sites form the first group, the T2-6-ring_2 and T4-6-ring_2 centers create the second group, and the third group is composed of the T1-6-ring_1, T3-6-ring_1, T1-8-ring_2, and T3-8-ring_2 sites.

6.3. Preferences of Na^+ for Various Rings. Table 1 reveals the preferences of Na^+ for the siting in rings of different sizes. In the case of Al-rich zeolites for which there are enough experimental data, all zeolite rings (except 4-rings) must serve as cationic sites for monovalent cations due to a high framework aluminum content. Regarding Si-rich zeolites, experimental data on the monovalent cation siting are available only for mordenite[8] and ZSM-5.[10−16] However, these data

https://doi.org/10.1021/acs.jpcc.2c02496
J. Phys. Chem. C 2022, 126, 10686−10702

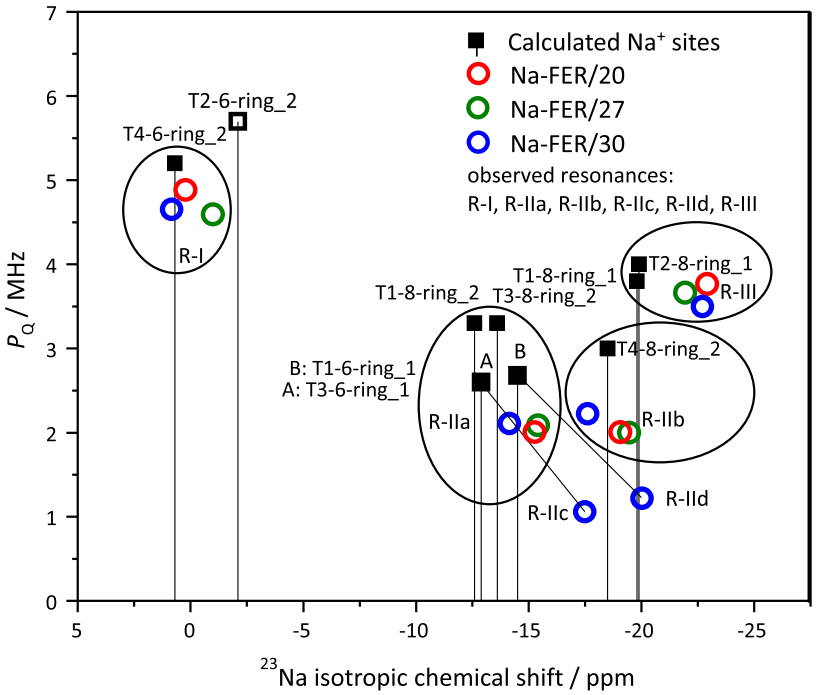

Figure 11. Comparison of the relationship between the calculated (squares) and observed (circles) nuclear quadrupolar coupling product (P_Q) and the calculated (squares) and observed (circles) ^{23}Na isotropic chemical shifts for the nine calculated Na^+ cationic sites. The black squares correspond to the cationic sites occupied by Na^+, while the white square relates to the most likely unoccupied cationic site.

cannot be directly employed for this purpose because of (i) the competition between the monovalent cations at a higher Al content due to a possible presence of Al_{PAIR} atoms,[34] (ii) the presence of only deformed 6-rings similar to 6-ring_1 of ferrierite (the α site for divalent cations when two Al atoms are present in the ring) for mordenite and ZSM-5, and (iii) the existence of 6-rings with different geometries than 6-ring_1 for ZSM-5. Only experimental data regarding the siting of divalent cations (with the exception of potassium-exchanged ferrierite[9] described below) are available for other Si-rich zeolites. The siting of divalent cations is governed by the presence of Al_{PAIR} atoms[34] in the rings on the surface of zeolite channels. The four crystallographically distinguishable framework T sites of the ferrierite framework belong to several ring types—5-rings, 6-rings, and 8-rings. However, 4-rings in the A zeolites are the exception, and the corresponding cationic sites are energetically disfavored compared to the sites formed by larger rings. Our DFT calculations using MD provided no Na^+ cationic sites created by 5-rings either, indicating that the siting of a larger cation as Na^+ is unfavorable also in this ring size. Table 1 shows the effect of the zeolite-ring size on the relative energy of the Na^+ cationic sites formed by the various rings with the Al atom in the same framework T site. It is clear that the cationic sites created by 6-ring_1 (Figure 2) and 6-ring_2 (Figure 4) are preferred compared to the sites formed by 8-ring_1 (Figure 1) and 8-ring_2 (Figure 3). The only exception is the sites connected with the Al(T1) atom as the Na^+ center formed by T1-8-ring_1 is the most stable one. This may be explained by the fact that Na^+ is positioned slightly above the plane of the oxygen atoms to which it is coordinated for T1-8-ring_1, while Na^+ is placed markedly above the plane of the oxygen atoms to which it is ligated for T1-6-ring_1 (Figure 5). Moreover, analogous results showing the preference for 6-rings relative to 8-rings were obtained for the Na^+ siting in SSZ-13 (CHA topology) in our prior study.[60]

A potassium-equilibrated ferrite sample was analyzed by neutron powder diffraction.[9] Two K(1) and K(2) potassium cationic sites were found, and furthermore, a third extra-framework species assigned to an oxygen atom, O(9), was determined. The K(1) center corresponds to the T1-8-ring_1 site for Na^+, while the K(2) extra-framework cation relates to no Na^+ site of our study. K(2) is located in 10-rings and is coordinated to two O atoms of an $Al(T2)O_4^-$ tetrahedron. Since the Si/Al ratio of the potassium-exchanged ferrierite is 8,[9] Al_{PAIR}[34] atoms are most likely present in the sample.[4,5] Since (i) Al pairs creating the β cationic sites predominate in ferrierites[5] and (ii) Al pairs forming these β sites are created only by the Al(T2)−Si−Si−Al(T2) sequences[38] (i.e., $\beta 2$[24]), the K(2) cations most likely balance the two Al atoms of the Al(T2)−Si−Si−Al(T2) sequences. Therefore, the K(2) cations are located in the 10-rings to maximize the distance between two K(2) cations. If O(9) was not an oxygen atom but a potassium cation, then this K^+ cationic site would be equal to the T3-8-ring_2 site of Na^+. These results show the opposite tendency of K^+ with respect to Na^+ to occupy 8-rings rather than 6-rings. Furthermore, analogous results show that the preference for 8-rings relative to 6-rings were gained for the K^+ siting in SSZ-13 (CHA topology) in our previous investigation.[60] Monovalent cations choose the ring type depending on their size. However, it should be noted that the energy stability of monovalent cations in cationic sites corresponding to a particular Al siting (i.e., thermodynamics) represents only one parameter controlling the occupation of the sites in the dehydrated zeolite. In the case of zeolites with a nonequivalent channel system (e.g., ferrierite with the main 10-ring channel and the side 8-ring channel), kinetics of the site occupation during the dehydration process as well as the starting locations of the solvated cations in the channel system of the hydrated zeolite (at the channel intersections in ferrierite zeolites) can play a role.

https://doi.org/10.1021/acs.jpcc.2c02496
J. Phys. Chem. C 2022, 126, 10686−10702

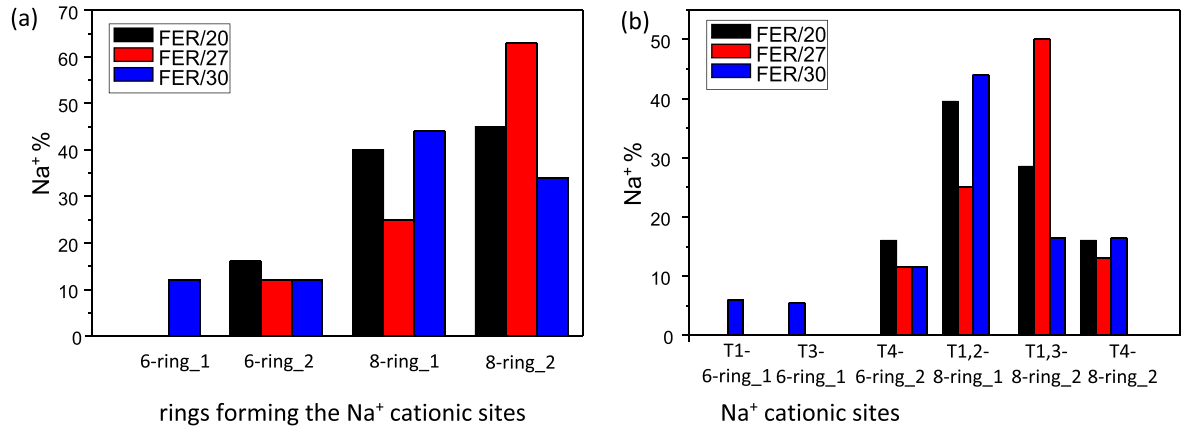

Figure 12. Relative concentrations of Na^+ cations (in %) in the (a) specific rings forming the Na^+ cationic sites and the (b) individual Na^+ cationic sites for the FER/20, FER/27, and FER/30 samples. The T2-6-ring_2 site is not occupied by Na^+ in the three samples.

6.4. Analysis of the Siting of Na^+ Cations in Si-Rich Ferrierite Matrices. Table 1 shows that there is no significant variability in the calculated values of the asymmetry parameter (η) since most sites feature η from ca. 0.5 to ca. 0.8. Table 2 reveals that the low sensitivity of η on the cation siting is further confirmed by the experimental results (η lying in the range from 0.6 to 0.7). Therefore, the combination of (i) the nuclear quadrupolar coupling product (P_Q), which describes the quadrupolar interaction using one number, and (ii) the ^{23}Na isotropic chemical shifts (δ_{iso}) for the individual sites is employed for the characterization of Na^+ cations in the individual centers. The relationship between the calculated and observed ^{23}Na isotropic chemical shifts (δ_{iso}) and the calculated and observed nuclear quadrupolar coupling product (P_Q) of Na^+ cations (Tables 1 and 2) is compared and shown in Figure 11.

It can be clearly seen that the calculated and experimental P_Q and δ_{iso} values are in very good agreement. Therefore, the combination of P_Q and δ_{iso} is essential for the full characterization of the Na^+ sites (it should be noted that η can be employed to serve as an additional parameter in specific cases, see below).

Figure 11 clearly shows three groups of the ^{23}Na NMR resonances—one R-I, four R-II (i.e., R-IIa, R-IIb, R-IIc, and R-IId), and one R-III. On the one hand, Table 1 and Figure 4 show that the ^{23}Na NMR resonance R-I with the most positive value of the observed δ_{iso} (between 1 and −2 ppm) clearly corresponds to Na^+ cations accommodated in 6-ring_2 of the ferrierite side channel. Most likely, the Al atoms balanced by these Na^+ cations are located in the framework T4 site as the calculated and observed NMR parameters are in significantly better agreement for Al(T4) than for Al(T2). On the other hand, Table 1 and Figure 1 show that the ^{23}Na NMR resonance R-III with the most negative value of the observed δ_{iso} (between −22 and −23 ppm) relates to Na^+ cations located in 8-ring_1. However, the experimental values of η (0.6−0.7) do not allow the determination whether either Al(T1) or Al(T2) or both Al(T1) and Al(T2) atoms form this cationic site.

The four R-II resonances have to correspond to Na^+ cations present in 6-ring_1 and 8-ring_2. The presence of all four R-II resonances in the spectra of the Na-FER/30 sample can be employed for the assignment of the four R-II resonances to the Na^+ cationic sites since each of the close four R-IIa—R-IId resonances unambiguously relates to one type of Na^+ siting. The ^{23}Na NMR resonances R-IIc and R-IId with low P_Q values correspond to Na^+ cations accommodated in 6-ring_1, most likely, the T3-6-ring_1 and T1-6-ring_1 sites, respectively. The large deviations of the observed values of the ^{23}Na isotropic chemical shifts of the R-IIc and R-IId resonances from the corresponding values predicted by DFT reflect rather the effect of the close ^{23}Na NMR resonances of a high intensity to those of a low intensity (i.e., R-IIc and R-IId) than a systematic discrepancy between the experimental and theoretical values of the ^{23}Na isotropic chemical shifts (compare the differences for the other ^{23}Na NMR resonances). The ^{23}Na NMR resonances R-IIa and R-IIb with high P_Q values can be assigned to Na^+ cation siting in 8-ring_2. However, there is uncertainty regarding the Al siting in 8-ring_2 for the two resonances. A comparison of the calculated and experimental NMR parameters gives two most likely assignments: (i) the ^{23}Na NMR resonance R-IIa with the observed ^{23}Na isotropic chemical shift at around −15 ppm relates to Na^+ cations located in both the T1-8-ring_2 and T3-8-ring_2 sites and the ^{23}Na NMR resonance R-IIb with the experimental ^{23}Na isotropic chemical shift at around −18 ppm correlates with the T4-8-ring_2 site or (ii) the ^{23}Na NMR resonances R-IIa and R-IIb could be identified with the T1-8-ring_2 and T3-8-ring_2 sites, respectively, and the T4-8-ring_2 site is not occupied by Na^+ cations. Nevertheless, the pattern of the experimental data shown in Figure 11 favors the former assignment with the ^{23}Na NMR resonance R-IIb belonging to the T4-8-ring_2 site. It should be noted that there is no uncertainty to which ring the R-IIb relates to (i.e., 8-ring_2), only the Al siting in 8-ring_2 is not fully certain. Our study shows that this Al siting cannot be determined by using exclusively ^{23}Na solid-state NMR spectroscopy but additional methods are required. The analysis of the Al siting in the framework T sites of the ferrierites studied[24] and/or the Li^+ siting in these matrices[6] can be employed for this purpose. Both the Al siting and Li^+ siting show that the framework T1 and T2 sites are not occupied in the FER/20 and FER/30 samples, respectively. This finding provides clues to assign the R-IIa and R-IIb as well as the R−III resonances.

The assignment of the ^{23}Na NMR resonances R-IIa and R-IIb to the T1-8-ring_2 and T3-8-ring_2 sites, respectively, would result in the presence of the Al atom in the T1 site in the FER/20 sample, which is not true. Therefore, the ^{23}Na NMR resonance R-IIa is unambiguously assigned to the Na^+ accommodated in the T1-8-ring_2 (FER/30) and T3-8-ring_2

https://doi.org/10.1021/acs.jpcc.2c02496
J. Phys. Chem. C 2022, 126, 10686−10702

Table 3. Al Relative Concentrations in the Crystallographically Distinguishable Tetrahedral Framework Sites (T sites) for the FER/20, FER/27, and FER/30 Samples

	Al concentration (in %) in the T sites													
	T1			T2			T3 + T4[a]		T3		T4		T3 + T4	
sample	Na[b]	Al[c]	Li[d]	Na[b]	Al[c]	Li[d]	Na[b]	Li[d]	Na[b]	Al[c]	Na[b]	Al[c]	Na[b]	Al[c]
FER/20	0–69	0	0	0–40	50	50	32–61	50	0–29	15	32	35	32–61	50
FER/27	0–76	5	5	0–26	30	35	24–74	60	0–50	20	24	45	24–74	65
FER/30	6–66	80	80	0–44	0	0	35–51	20	6–22	5	29	15	35–51	20

[a]^{7}Li NMR did not allow the selection between Al in the T3 and T4 sites. [b]Al relative concentration estimated using ^{23}Na MAS NMR. [c]Al relative concentration estimated using ^{27}Al MAS NMR. The data are taken from ref 24. [d]Al relative concentration estimated using ^{7}Li MAS NMR. The data are taken from ref 6.

(FER/20 and FER/27) sites, while the ^{23}Na NMR resonance R-IIb reflects the Na^+ located at the T4-8-ring_2 site. Similarly, the ^{23}Na NMR resonance R-I must correspond to Na^+ located in the T4-6-ring_2 site and not in the T2-6-ring_2 center since Al(T2) atoms are not present in the FER/30 sample.

Employing the absence of Al(T1) in the FER/20 sample and a very low concentration of Al(T1) in the FER/27 sample on the one hand, and the absence of Al(T2) in the FER/30 sample on the other hand, we can assign the ^{23}Na NMR resonance R-III to the T2-8-ring_1 site for FER/20 and FER/27, while R-III belongs to the T1-8-ring_1 site for FER/30.

The quantitative distribution of Na^+ cations accommodated in the individual cationic sites for all the three samples is shown in Figure 12. Figure 12a shows the siting of Na^+ cations in the specific rings creating the Na^+ cationic sites, while Figure 12b shows the detailed Na^+ distribution in the individual Na^+ cationic sites including the Al siting in the ring forming the corresponding Na^+ cationic sites. Figure 12 clearly shows that the ferrierite zeolites even with rather close Si/Al ratios between 20 and 30 exhibit significant differences in the Na^+ siting, confirming that the Al organization (for definition of the Al organization, see ref 34) and not the Si/Al ratio is the key determining factor for understanding the catalyst performance. On the one hand, 6-ring_1 is occupied only in the FER/30 sample. On the other hand, the remaining three rings are occupied in all the samples. The occupancy of Na^+ cations is similar for 6-ring_2, while it significantly varies for 8-ring_1 and 8-ring_2. Figure 12b shows that the FER/20 and FER/30 samples exhibit similar Na^+ relative concentrations in the individual cationic sites formed by 6-ring_2, 8-ring_1, and 8-ring_2. The Na^+ occupancies in the FER/27 zeolite markedly differ (differences up to 90 relative %) in comparison with the FER/20 and FER/30 samples for the two sites formed by 8-ring_1 with Al(T1) and Al(T2) (i.e., the T1,2-8-ring_1 sites) and the two sites created by 8-ring_2 with Al(T1) and Al(T3) (i.e., the T1,3-8-ring_2 sites), while the Na^+ relative concentrations are similar for all the three samples for the T4-6-ring_2 and T4-8-ring_2 sites.

As it has been mentioned in the previous paragraphs, while the individual resonances can be unambiguously assigned to the zeolite rings forming the Na^+ cationic sites, there is uncertainty regarding the relationship between the ^{23}Na NMR resonances and the Al siting in these rings (Al(T1) + Al(T2) for 8-ring_1 and Al(T1) + Al(T3) for 8-ring_2). This results in a huge variability of possible Al relative concentrations in the individual T sites when estimated solely from the Na^+ siting (a variability in the range from 0 to 76% of Al atoms in a T site). Only the concentration of Al atoms in the T4 site can be estimated for the investigated samples. Therefore, the application of Na^+ cations as probes for the Al siting is significantly limited. Conversely, the results of our prior studies concerning the Al siting[24] and the Li^+ siting[6] in the three ferrierite samples can be employed for the verification of the analysis of the Na^+ siting in the same three ferrierite samples. The Al relative concentrations in the individual T sites estimated using ^{23}Na, ^{27}Al, and ^{7}Li solid-state NMR experiments are compared in Table 3. It should be noted that the ^{7}Li NMR measurements did not permit the selection between Al(T3) and Al(T4) atoms, and therefore, the Al relative concentrations for both the Al(T3) and Al(T4) atoms together are included in Table 3.

Table 3 shows that there are mainly only small discrepancies between the Al relative concentrations in the individual T sites estimated using ^{23}Na, ^{27}Al, and ^{7}Li solid-state NMR experiments. Negligible or low concentrations of Al atoms in (i) the T1 site for FER/20 and FER/27 and (ii) the T2 site for FER/30 are not in conflict with the results of the ^{23}Na NMR experiments according to which the Al relative concentration can vary, depending on the assignment of the ^{23}Na NMR resonances, between 0 and 76% for Al(T1) and 0 and 44% for Al(T2). The largest discrepancies between the relative concentrations obtained from, on the one hand, ^{23}Na solid-state NMR measurements and, on the other hand, ^{27}Al solid-state NMR experiments are for the T4 sites for the FER/27 sample. This inaccuracy can be explained either by the fact that the overlapping ^{23}Na NMR resonances R-IIa and R-IIb with close NMR parameters are employed or there is a more pronounced error in the analysis of the Al siting of that sample using ^{27}Al MAS NMR. It should be noted that ^{27}Al MAS NMR spectra of all the three ferrierite samples are formed by closely overlapping ^{27}Al NMR resonances, and the ^{27}Al NMR parameters for simulations of the ^{27}Al MAS NMR spectra for the quantitative analysis were estimated using a visual inspection of the ^{27}Al MQMAS NMR spectra.[24] Nevertheless, as it has been concluded above, ^{23}Na solid-state NMR spectroscopy represents a powerful tool for the analysis of the Na^+ siting in zeolite rings (i.e., the identification of the rings with an Al atom). Therefore, ^{23}Na (MQ)MAS NMR can be suggested as a supporting method for the analysis of the Al siting in zeolite matrices.

Taking into account that the T1 site is not occupied by Al atoms in the FER/20 sample and has a very low occupancy in the FER/27 matrix, the ^{23}Na NMR resonances R-III and R-IIa assigned to the cationic sites formed by 8-ring_1 and 8-ring_2, respectively, in these samples have the Al atoms located in the T2 and T3 sites, respectively. Conversely, the T2 site is not occupied by Al and the T3 site has a very low Al occupancy in the FER/30 sample, and therefore, the ^{23}Na NMR resonances R-III and R-IIa relate to the sites formed by 8-ring_1 and 8-ring_2, respectively, with Al atoms in the T1 site. Thus, the

https://doi.org/10.1021/acs.jpcc.2c02496
J. Phys. Chem. C 2022, 126, 10686−10702

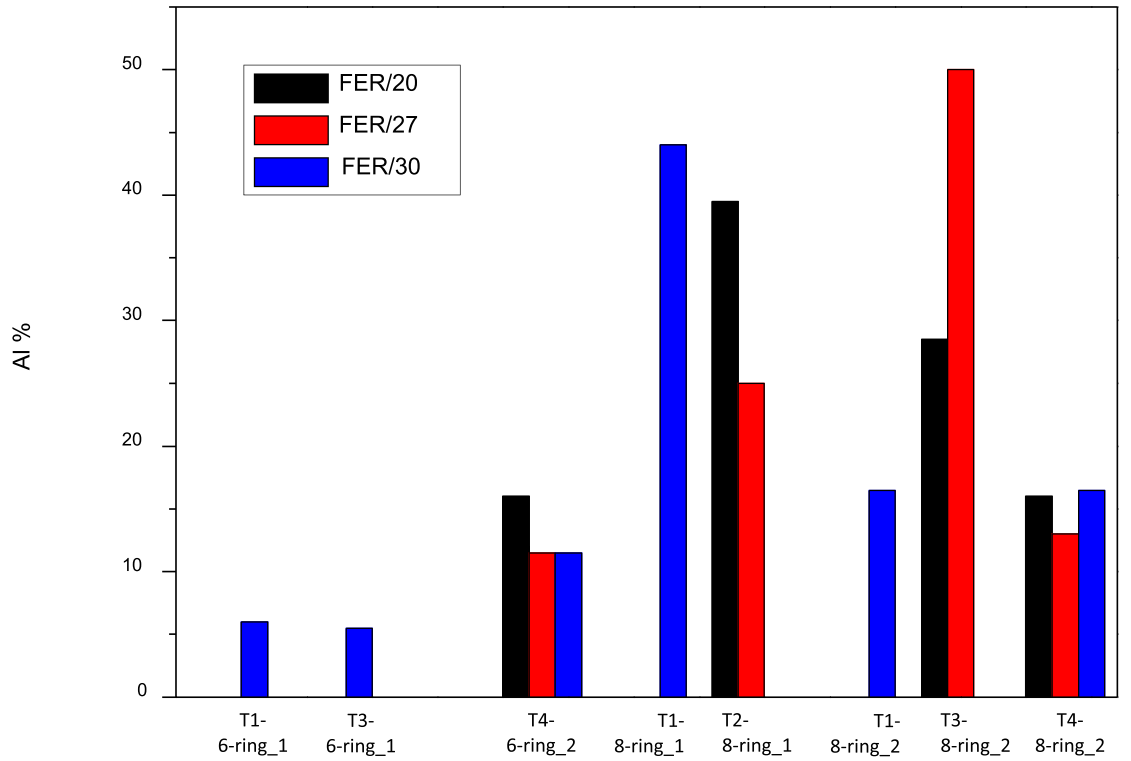

Figure 13. Relative concentrations of Al atoms (in %) corresponding to the individual Na^+ cationic sites for the FER/20, FER/27, and FER/30 samples. There are no Al atoms forming the T2-6-ring_2 site in the three samples.

unambiguous analysis of the Na^+ siting in the investigated samples can be estimated using the combination of the ^{23}Na solid-state NMR experiments with the support of ^{7}Li and ^{27}Al solid-state NMR measurements (Figure 13). These results clearly provide evidence that the Na^+ sitings in the three ferrierite samples significantly differ. Figure 13 shows that even when only the Na^+ siting in the rings is taken into account, it markedly varies in the three samples. The FER/30 sample exhibits similarities with the FER/20 and FER/27 matrices only in the Na^+ siting in the T4-6-ring_2 and T4-8-ring_2 sites. Conversely, the Na^+ siting in the 8-ring_1 and 8-ring_2 (except for T4-8-ring_2) sites differs not only quantitatively, but also by the T site occupied by Al atom (the T1 vs T2 site for 8-ring_1 and the T1 vs T3 for 8-ring_2). These marked differences clearly reflect the various Al sitings in the three investigated samples. This is significantly different with respect to the siting of bare divalent cations in Si-rich zeolites with Al pairs. In this case, the concentration of Al pairs is reflected in the maximum possible concentration of bare cations in the zeolite and varies, but the relative distributions of bare cations in the maximum loaded samples in the α, β, and γ sites[24] do not exhibit a significant variability. The β site significantly predominates (typically around 60% of the cations in the maximum loaded sample followed by the α site with 20—35% of the cations for, e.g., ZSM-5, ferrierite, mordenite, and beta zeolite).[4,5]

Surprisingly, there is a marked discrepancy between the occupation of the Na^+ cationic sites (Figure 13) and their calculated relative energies (Table 1). Only for Al(T1), the most stable T1-8-ring_1 site is preferentially occupied by Na^+, while the Na^+ occupancy of the other two low energy sites T1-6-ring_1 and T1-8-ring_2 is lower. Conversely, for Al(T2), only the less stable (by 4 kcal/mol) T2-8-ring_1 cationic site is occupied by Na^+ (Figure 13). Similarly, for Al(T3), the T3-8-ring_2 site, which is higher in energy by 4 kcal/mol, is preferentially occupied by Na^+ in comparison with the more stable T3-6-ring_1 site. For Al(T4), both T4-6-ring_2 and T4-8-ring_2 feature comparable occupancies by Na^+ although the former is lower in energy by 7 kcal/mol than the latter. These results clearly provide evidence for a significant role of the starting positions of the Na^+ cations in the hydrated zeolite and the kinetics of the occupation of the Na^+ cationic sites during the dehydration process. It is especially difficult for the Na^+ cations to be accommodated in the 6-ring_2 sites. Therefore, the siting of monovalent cations in extra-framework cationic sites cannot be predicted from the known Al siting in the zeolite matrix of interest and the calculated relative energies but must be determined experimentally.

7. CONCLUSIONS

A method for the analysis of the siting of monovalent Na^+ cations in extra-framework cationic sites in Si-rich ferrierite zeolites was developed. The Na^+ siting was analyzed by a combination of high-field (500 MHz) and ultra-high-field (900 MHz) MAS and MQMAS ^{23}Na NMR spectroscopy interpreted using predictions of the ^{23}Na NMR parameters obtained from periodic DFT calculations including extensive MD simulations. The employment of high-field and ultra-high-field ^{23}Na solid-state NMR allows estimations of the ^{23}Na NMR parameters of Na^+ cations in different cationic sites with a high reliability. On the one hand, ^{23}Na MAS NMR spectroscopy is essential for the identification of Na^+ cations with a high quadrupolar broadening. ^{23}Na NMR resonances of such cations are suppressed in ^{23}Na MQMAS NMR experiments. On the other hand, ^{23}Na MQMAS NMR measurements

https://doi.org/10.1021/acs.jpcc.2c02496
J. Phys. Chem. C 2022, 126, 10686−10702

are essential for the analysis of close overlapping resonances with a lower quadrupolar broadening.

Our study of ferrierite matrices with isolated framework Al atoms reveals that Na^+ cations can occupy nine distinct extra-framework cationic sites formed by two 6-rings and two 8-rings with one Al atom located in different framework T sites. 5-rings do not create cationic sites for Na^+ cations. The Na^+ is positioned highly asymmetrically in 8-ring_1 and is slightly above the plane of the oxygen atoms to which it is coordinated for the T1-8-ring_1 and T2-8-ring_1 cationic sites formed by the Si(T2)-Si(T2)-Al(T1)-Si(T1)-Si(T2)-Si(T2)-Si(T1)-Si-(T1) and Al(T2)-Si(T2)-Si(T1)-Si(T1)-Si(T2)-Si(T2)-Si-(T1)-Si(T1) sequences, respectively. Na^+ is placed approximately symmetrically in 6-ring_1 and is markedly above the plane of the oxygen atoms to which it is ligated for the T1-6-ring_1 and T3-6-ring_1 cationic sites created by the Al(T1)-Si(T1)-Si(T3)-Si(T1)-Si(T1)-Si(T3) and Si(T1)-Si(T1)-Al-(T3)-Si(T1)-Si(T1)-Si(T3) chains, respectively. The Na^+ cation is located roughly symmetrically (T1-8-ring_2 and T3-8-ring_2) and very asymmetrically (T4-8-ring_2) in 8-ring_2 and is well above the plane of the oxygen atoms to which it is bound for the T1-8-ring_2, T3-8-ring_2, and T4-8-ring_2 cationic sites made of the Si(T4)-Si(T2)-Al(T1)-Si(T1)-Si(T2)-Si(T4)-Si(T3)-Si(T3), Si(T4)-Si(T2)-Si(T1)-Si(T1)-Si(T2)-Si(T4)-Al(T3)-Si(T3), and Al(T4)-Si(T2)-Si-(T1)-Si(T1)-Si(T2)-Si(T4)-Si(T3)-Si(T3) sequences, respectively. 6-ring_2 constitutes two (near) planar cationic sites with a high symmetry, that is, the T2-6-ring_2 and T4-6-ring_2 centers built of the Al(T2)-Si(T2)-Si(T4)-Si(T2)-Si(T2)-Si(T4) and Si(T2)-Si(T2)-Al(T4)-Si(T2)-Si(T2)-Si-(T4) chains, respectively. The cationic sites created by 8-ring_1 and 6-ring_1 are accessible through the 10-rings while those formed by 8-ring_2 and 6-ring_2 are reachable through 8-ring_1.

Both the theoretical and experimental results show that the ^{23}Na NMR parameters are sensitive to the cation coordination, which in turn reflects the structure of the ring forming the corresponding cationic site. Although the detailed arrangement of the Na^+ in the cationic site as well as the corresponding ^{23}Na NMR parameters can be predicted only employing quantum chemical calculations, some empirical conclusions can be made. Highly asymmetric but approximately planar Na^+ cationic sites, that is, T1-8-ring_1 and T2-8-ring_1, feature the most negative (ca. −20 ppm) ^{23}Na isotropic chemical shift and a C_Q of 3.7 MHz. The (near) planar Na^+ cationic sites with a high symmetry, that is, T2-6-ring_2 and T4-6-ring_2, have the least negative or even a positive (ca. 0 ppm) ^{23}Na isotropic chemical shift and the highest C_Q of ca. 5 MHz. The sites with the Na^+ cation located well above the plane of the oxygen atoms to which it is bonded, that is, T1-6-ring_1, T3-6-ring_1, T1-8-ring_2, T3-8-ring_2, and T4-8-ring_2, possess ^{23}Na isotropic chemical shifts ranging from −13 to −15 ppm, with the exception (−19 ppm) of the T4-8-ring_2 site due to its highly asymmetric coordination, and C_Q values ranging from 2.4 to 3.0 MHz.

The Al siting in the rings forming the Na^+ cationic sites is not markedly reflected in the Na^+ coordination and thus in the corresponding ^{23}Na NMR parameters. Therefore, ^{23}Na solid-state NMR spectroscopy can clearly identify the ring accommodating the Na^+ cation, while the Al siting in the ring can be determined solely for some specific cases [i.e., Al(T4)]. However, ^{23}Na solid-state NMR spectroscopy together with an additional method sensitive to the Al siting in the zeolite matrix (e.g., ^{27}Al solid-state NMR and ^{7}Li solid-state NMR) can resolve both the ring forming the Na^+ cationic site and the corresponding Al siting in the ring.

Eight of the nine predicted Na^+ cationic sites are occupied by Na^+ in one or more of the investigated samples. Only T2-6-ring_2 is empty in all the three studied samples. However, the Na^+ relative concentration in the individual cationic sites of the three differently synthesized ferrierite samples significantly varies. Although the calculated relative energies are, with the exception of the T1-8-ring_1 site, lower for the Na^+ cationic sites created by the two 6-rings, the two 8-rings are preferentially occupied by Na^+ in the three dehydrated samples, clearly evidencing a significant role of the starting positions of the Na^+ cations in the hydrated zeolite and the kinetics of the occupation of the Na^+ cationic sites during the dehydration process. Therefore, quantum chemical calculations of the relative energies of extra-framework cationic sites cannot alone predict the siting of monovalent cations in the zeolite matrix of interest even when the corresponding Al siting is known.

Our study shows that ^{23}Na solid-state NMR spectroscopy represents, on the one hand, a highly promising tool for the analysis of the siting of monovalent cations in Si-rich zeolite matrices, and, on the other hand, a method permitting the identification of the rings with an Al atom, and when applied together with ^{27}Al and ^{7}Li solid-state NMR spectroscopies, it may allow the full analysis of the Al siting in Si-rich zeolites with a high number of framework T sites.

AUTHOR INFORMATION

Corresponding Author

Stepan Sklenak − *J. Heyrovský Institute of Physical Chemistry, The Czech Academy of Sciences, 18223 Prague, Czech Republic*; orcid.org/0000-0003-4862-857X; Email: stepan.sklenak@jh-inst.cas.cz

Authors

Petr Klein − *J. Heyrovský Institute of Physical Chemistry, The Czech Academy of Sciences, 18223 Prague, Czech Republic*

Jiri Dedecek − *J. Heyrovský Institute of Physical Chemistry, The Czech Academy of Sciences, 18223 Prague, Czech Republic*

Haunani M. Thomas − *J. Heyrovský Institute of Physical Chemistry, The Czech Academy of Sciences, 18223 Prague, Czech Republic*

Sarah R. Whittleton − *J. Heyrovský Institute of Physical Chemistry, The Czech Academy of Sciences, 18223 Prague, Czech Republic*

Jiri Klimes − *J. Heyrovský Institute of Physical Chemistry, The Czech Academy of Sciences, 18223 Prague, Czech Republic; Department of Chemical Physics and Optics, Charles University, 121 16 Prague 2, Czech Republic*

Jiri Brus − *Institute of Macromolecular Chemistry, The Czech Academy of Sciences, 162 06 Prague 6, Czech Republic*; orcid.org/0000-0003-2692-612X

Libor Kobera − *Institute of Macromolecular Chemistry, The Czech Academy of Sciences, 162 06 Prague 6, Czech Republic*; orcid.org/0000-0002-8826-948X

David L. Bryce − *Department of Chemistry and Biomolecular Sciences, University of Ottawa, Ottawa, Ontario K1N 6N5, Canada*; orcid.org/0000-0001-9989-796X

Complete contact information is available at: https://pubs.acs.org/10.1021/acs.jpcc.2c02496

https://doi.org/10.1021/acs.jpcc.2c02496
J. Phys. Chem. C 2022, 126, 10686−10702

Notes

The authors declare no competing financial interest.

■ ACKNOWLEDGMENTS

This work was supported by the Grant Agency of the Czech Republic # 19-05259S, RVO:61388955, and RVO:61389013 and by the Czech Academy of Sciences (Strategy AV21—Program Molecules and Materials for Life). This work was supported by the Ministry of Education, Youth and Sports of the Czech Republic through the e-INFRA CZ (ID:90140). D.L.B. thanks NSERC for funding. Access to the 21.1 T NMR spectrometer was provided by the National Ultrahigh-Field NMR Facility for Solids (Ottawa, Canada), a national research facility funded by a consortium of Canadian Universities, supported by the National Research Council Canada and Bruker BioSpin, and managed by the University of Ottawa (http://nmr900.ca).

■ REFERENCES

(1) Martínez, C.; Corma, A. Inorganic molecular sieves: Preparation, modification and industrial application in catalytic processes. *Coord. Chem. Rev.* **2011**, *255*, 1558−1580.
(2) Ennaert, T.; Van Aelst, J.; Dijkmans, J.; De Clercq, R.; Schutyser, W.; Dusselier, M.; Verboekend, D.; Sels, B. F. Potential and challenges of zeolite chemistry in the catalytic conversion of biomass. *Chem. Soc. Rev.* **2016**, *45*, 584−611.
(3) Suganuma, S.; Katada, N. Innovation of catalytic technology for upgrading of crude oil in petroleum refinery. *Fuel Process. Technol.* **2020**, *208*, 106518.
(4) Dedecek, J.; Sobalik, Z.; Wichterlova, B. Siting and distribution of framework aluminium atoms in silicon-rich zeolites and impact on catalysis. *Catal. Rev.: Sci. Eng.* **2012**, *54*, 135−223.
(5) Dedecek, J.; Tabor, E.; Sklenak, S. Tuning the aluminum distribution in zeolites to increase their performance in acid-catalyzed reactions. *ChemSusChem* **2019**, *12*, 556−576.
(6) Klein, P.; Dedecek, J.; Thomas, H. M.; Whittleton, S. R.; Pashkova, V.; Brus, J.; Kobera, L.; Sklenak, S. NMR crystallography of monovalent cations in inorganic matrixes: Li^+ siting and the local structure of Li^+ sites in ferrierites. *Chem. Commun.* **2015**, *51*, 8962−8965.
(7) http://www.iza-structure.org/databases/ (accessed April 25, 2021).
(8) Mortier, W. J. *Extraframework Cationic Positions in Zeolites*; Elsevier: Amsterdam, 1982.
(9) Pickering, I.; Maddox, P. J.; Thomas, J. M.; Cheetham, A. K. A neutron powder diffraction analysis of potassium-exchanged ferrierite. *J. Catal.* **1989**, *119*, 261−265.
(10) Mentzen, B. F. Crystallographic determination of the positions of the monovalent H, Li, Na, K, Rb, and Tl cations in fully dehydrated MFI type zeolites. *J. Phys. Chem. C* **2007**, *111*, 18932−18941.
(11) Mentzen, B. F.; Bergeret, G. Crystallographic determination of the positions of the copper cations in zeolite MFI. *J. Phys. Chem. C* **2007**, *111*, 12512−12516.
(12) Lin, J.-C.; Chao, K.-J.; Wang, Y. The location of cations in Cs-exchanged ZSM-5 zeolite. *Zeolites* **1991**, *11*, 376−379.
(13) Olson, D. H.; Khosrovani, N.; Peters, A. W.; Toby, B. H. Crystal structure of dehydrated CsZSM-5 (5.8 Al): Evidence for nonrandom aluminum distribution. *J. Phys. Chem. B* **2000**, *104*, 4844−4848.
(14) Mentzen, B. F.; Bergeret, G.; Emerich, H.; Weber, H.-P. Dehydrated and Cs^+-exchanged MFI zeolites: Location and population of Cs^+ from in situ diffraction data as a function of temperature and degree of exchange. *J. Phys. Chem. B* **2006**, *110*, 97−106.
(15) Kim, C. W.; Heo, N. H.; Seff, K. Framework sites preferred by aluminum in zeolite ZSM-5. Structure of a fully dehydrated, fully Cs^+-exchanged ZSM-5 crystal (MFI, Si/Al=24). *J. Phys. Chem. C* **2011**, *115*, 24823−24838.
(16) Heo, N. H.; Kim, C. W.; Kwon, H. J.; Kim, G. H.; Kim, S. H.; Hong, S. B.; Seff, K. Detailed determination of the Tl^+ positions in zeolite Tl-ZSM-5. Single-crystal structures of fully dehydrated Tl-ZSM-5 and H-ZSM-5 (MFI, Si/Al=29). Additional evidence for a nonrandom distribution of framework aluminum. *J. Phys. Chem. C* **2009**, *113*, 19937−19956.
(17) Koller, H.; Burger, B.; Schneider, A. M.; Engelhardt, G.; Weitkamp, J. Location of Na^+ and Cs^+ cations in CsNaY zeolites studied by ^{23}Na and ^{133}Cs magic-angle spinning nuclear magnetic resonance spectroscopy combined with X-ray structure analysis by Rietveld refinement. *Microporous Mater.* **1995**, *5*, 219−232.
(18) Feuerstein, M.; Hunger, M.; Engelhardt, G.; Amoureux, J. P. Characterisation of sodium cations in dehydrated zeolite NaX by ^{23}Na NMR spectroscopy. *Solid State Nucl. Magn. Reson.* **1996**, *7*, 95−103.
(19) Abraham, K. M. How comparable are sodium-ion batteries to lithium-ion counterparts? *ACS Energy Lett.* **2020**, *5*, 3544−3547.
(20) Zukal, A.; Zones, S. I.; Kubů, M.; Davis, T. M.; Čejka, J. Adsorption of carbon dioxide on sodium and potassium forms of STI zeolite. *ChemPlusChem* **2012**, *77*, 675−681.
(21) Frantz, T. S.; Ruiz, W. A.; da Rosa, C. A.; Mortola, V. B. Synthesis of ZSM-5 with high sodium content for CO_2 adsorption. *Microporous Mesoporous Mater.* **2016**, *222*, 209−217.
(22) Arletti, R.; Gigli, L.; di Renzo, F.; Quartieri, S. Evidence for the formation of stable CO_2 hydrates in zeolite Na-Y: Structural characterization by synchrotron X-ray powder diffraction. *Microporous Mesoporous Mater.* **2016**, *228*, 248−255.
(23) Cheung, O.; Bacsik, Z.; Fil, N.; Krokidas, P.; Wardecki, D.; Hedin, N. Selective adsorption of CO_2 on zeolites NaK-ZK-4 with Si/Ai of 1.8-2.8. *ACS Omega* **2020**, *5*, 25371−25380.
(24) Dedecek, J.; Lucero, M. J.; Li, C. B.; Gao, F.; Klein, P.; Urbanova, M.; Tvaruzkova, Z.; Sazama, P.; Sklenak, S. Complex analysis of the aluminum siting in the framework of silicon-rich zeolites. A case study on ferrierites. *J. Phys. Chem. C* **2011**, *115*, 11056−11064.
(25) Space group: Immm; Cell parameters: a = 19.018 Å, b = 14.303 Å, c = 7.541 Å. http://www.iza-structure.org/databases/ (accessed April 25, 2021).
(26) VandeVondele, J.; Krack, M.; Mohamed, F.; Parrinello, M.; Chassaing, T.; Hutter, J. QUICKSTEP: Fast and accurate density functional calculations using a mixed Gaussian and plane waves approach. *Comput. Phys. Commun.* **2005**, *167*, 103−128.
(27) The CP2K developers group. https://cp2k.org/ (accessed April 25, 2021).
(28) Becke, A. D. Density-functional exchange-energy approximation with correct asymptotic-behavior. *Phys. Rev. A* **1988**, *38*, 3098−3100.
(29) Lee, C.; Yang, W.; Parr, R. G. Development of the Colle-Salvetti correlation-energy formula into a functional of the electron-density. *Phys. Rev. B: Condens. Matter Mater. Phys.* **1988**, *37*, 785−789.
(30) Hartwigsen, C.; Goedecker, S.; Hutter, J. Relativistic separable dual-space Gaussian pseudopotentials from H to Rn. *Phys. Rev. B: Condens. Matter Mater. Phys.* **1998**, *58*, 3641−3662.
(31) Krack, M. Pseudopotentials for H to Kr optimized for gradient-corrected exchange-correlation functionals. *Theor. Chem. Acc.* **2005**, *114*, 145−152.
(32) Sklenak, S.; Andrikopoulos, P. C.; Whittleton, S. R.; Jirglova, H.; Sazama, P.; Benco, L.; Bucko, T.; Hafner, J.; Sobalik, Z. Effect of the Al siting on the structure of Co(II) and Cu(II) cationic sites in ferrierite. A periodic DFT molecular dynamics and FTIR study. *J. Phys. Chem. C* **2013**, *117*, 3958−3968.
(33) Tabor, E.; Lemishka, M.; Sobalik, Z.; Mlekodaj, K.; Andrikopoulos, P. C.; Dedecek, J.; Sklenak, S. Low-temperature selective oxidation of methane over distant binuclear cationic centers in zeolites. *Commun. Chem.* **2019**, *2*, 71.
(34) Mlekodaj, K.; Dedecek, J.; Pashkova, V.; Tabor, E.; Klein, P.; Urbanova, M.; Karcz, R.; Sazama, P.; Whittleton, S. R.; Thomas, H. M.; Fishchuk, A. V.; Sklenak, S. Al organization in the SSZ-13 zeolite.

https://doi.org/10.1021/acs.jpcc.2c02496
J. Phys. Chem. C 2022, 126, 10686−10702

Al distribution and extraframework sites of divalent cations. *J. Phys. Chem. C* **2019**, *123*, 7968−7987.
(35) Tabor, E.; Dedecek, J.; Mlekodaj, K.; Sobalik, Z.; Andrikopoulos, P. C.; Sklenak, S. Dioxygen dissociation over man-made system at room temperature to form the active Alpha-oxygen for methane oxidation. *Sci. Adv.* **2020**, *6*, eaaz9776.
(36) Sazama, P.; Moravkova, J.; Sklenak, S.; Vondrova, A.; Tabor, E.; Sadovska, G.; Pilar, R. Effect of the nuclearity and coordination of Cu and Fe sites in beta zeolites on the oxidation of hydrocarbons. *ACS Catal.* **2020**, *10*, 3984−4002.
(37) Dedecek, J.; Tabor, E.; Andrikopoulos, P. C.; Sklenak, S. Splitting dioxygen over distant binuclear transition metal cationic sites in zeolites. Effect of the transition metal cation. *Int. J. Quantum Chem.* **2021**, *121*, e26611.
(38) Tabor, E.; Lemishka, M.; Olszowka, J. E.; Mlekodaj, K.; Dedecek, J.; Andrikopoulos, P. C.; Sklenak, S. Splitting dioxygen over distant binuclear Fe sites in zeolites. Effect of the local arrangement and framework topology. *ACS Catal.* **2021**, *11*, 2340−2355.
(39) Kresse, G.; Hafner, J. Ab-initio molecular-dynamics for open-shell transition-metals. *Phys. Rev. B: Condens. Matter Mater. Phys.* **1993**, *48*, 13115−13118.
(40) Kresse, G.; Hafner, J. Ab-initio molecular-dynamics simulation of the liquid-metal amorphous-semiconductor transition in germanium. *Phys. Rev. B: Condens. Matter Mater. Phys.* **1994**, *49*, 14251−14269.
(41) Kresse, G.; Furthmüller, J. Efficiency of ab-initio total energy calculations for metals and semiconductors using a plane-wave basis set. *Comput. Mater. Sci.* **1996**, *6*, 15−50.
(42) Kresse, G.; Furthmüller, J. Efficient iterative schemes for ab initio total-energy calculations using a plane-wave basis set. *Phys. Rev. B: Condens. Matter Mater. Phys.* **1996**, *54*, 11169−11186.
(43) Harl, J.; Kresse, G. Cohesive energy curves for noble gas solids calculated by adiabatic connection fluctuation-dissipation theory. *Phys. Rev. B: Condens. Matter Mater. Phys.* **2008**, *77*, 045136.
(44) Kaltak, M.; Klimeš, J.; Kresse, G. Low scaling algorithms for the random phase approximation: Imaginary time and Laplace transformations. *J. Chem. Theory Comput.* **2014**, *10*, 2498−2507.
(45) Kaltak, M.; Klimes, J.; Kresse, G. Cubic scaling algorithm for the random phase approximation: Self-interstitials and vacancies in Si. *Phys. Rev. B: Condens. Matter Mater. Phys.* **2014**, *90*, 054115.
(46) Perdew, J. P.; Burke, K.; Ernzerhof, M. Generalized gradient approximation made simple. *Phys. Rev. Lett.* **1996**, *77*, 3865−3868.
(47) Ren, X.; Tkatchenko, A.; Rinke, P.; Scheffler, M. Beyond the random-phase approximation for the electron correlation energy: The importance of single excitations. *Phys. Rev. Lett.* **2011**, *106*, 153003.
(48) Klimeš, J.; Kaltak, M.; Maggio, E.; Kresse, G. Singles correlation energy contributions in solids. *J. Chem. Phys.* **2015**, *143*, 102816.
(49) Frisch, M. J.; et al. *Gaussian 09*, Revision C.01; Gaussian, Inc.: Wallingford CT, 2011.
(50) Adiga, S.; Aebi, D.; Bryce, D. L. EFGShield - A program for parsing and summarizing the results of electric field gradient and nuclear magnetic shielding tensor calculations. *Can. J. Chem.* **2007**, *85*, 496−505.
(51) Wolinski, K.; Hinton, J. F.; Pulay, P. Efficient implementation of the gauge-independent atomic orbital method for NMR chemical-shift calculations. *J. Am. Chem. Soc.* **1990**, *112*, 8251−8260.
(52) Becke, A. D. Density-functional thermochemistry. III. The role of exact exchange. *J. Chem. Phys.* **1993**, *98*, 5648−5652.
(53) Jensen, F. Basis set convergence of nuclear magnetic shielding constants calculated by density functional methods. *J. Chem. Theory Comput.* **2008**, *4*, 719−727.
(54) Baltisberger, J. H.; Xu, Z.; Stebbins, J. F.; Wang, S. H.; Pines, A. Triple-quantum two-dimensional ^{27}Al magic-angle spinning nuclear magnetic resonance spectroscopic study of aluminosilicate and aluminate crystals and glasses. *J. Am. Chem. Soc.* **1996**, *118*, 7209−7214.
(55) Mähler, J.; Persson, I. A study of the hydration of the alkali metal ions in aqueous solution. *Inorg. Chem.* **2012**, *51*, 425−438.
(56) Olson, D. H. The crystal-structure of dehydrated NaX. *Zeolites* **1995**, *15*, 439−443.
(57) Amoureux, J.-P.; Fernandez, C.; Steuernagel, S. Z filtering in MQMAS NMR. *J. Magn. Reson., Ser. A* **1996**, *123*, 116−118.
(58) Massiot, D.; Fayon, F.; Capron, M.; King, I.; Le Calvé, S.; Alonso, B.; Durand, J.-O.; Bujoli, B.; Gan, Z.; Hoatson, G. Modelling one- and two-dimensional solid-state NMR spectra. *Magn. Reson. Chem.* **2002**, *40*, 70−76.
(59) MacKenzie, K. J. D.; Smith, M. E. *Multinuclear Solid-State NMR of Inorganic Materials*; Pergamon: Oxford, U.K., 2002.
(60) Klein, P.; Pashkova, V.; Thomas, H. M.; Whittleton, S. R.; Brus, J.; Kobera, L.; Dedecek, J.; Sklenak, S. Local structure of cationic sites in dehydrated zeolites inferred from ^{27}Al magic-angle spinning NMR and density functional theory calculations. A study on Li-, Na-, and K-chabazite. *J. Phys. Chem. C* **2016**, *120*, 14216−14225.
(61) Czjzek, G.; Fink, J.; Götz, F.; Schmidt, H.; Coey, J. M. D.; Rebouillat, J.-P.; Liénard, A. Atomic coordination and the distribution of electric-field gradients in amorphous solids. *Phys. Rev. B: Condens. Matter Mater. Phys.* **1981**, *23*, 2513−2530.
(62) Dalconi, M. C.; Cruciani, G.; Alberti, A.; Ciambelli, P.; Rapacciuolo, M. T. Ni^{2+} ion sites in hydrated and dehydrated forms of Ni-exchanged zeolite ferrierite. *Microporous Mesoporous Mater.* **2000**, *39*, 423−430.
(63) Dalconi, M. C.; Alberti, A.; Cruciani, G. Cation migration and structural modification of Co-exchanged ferrierite upon heating: A time-resolved X-ray powder diffraction study. *J. Phys. Chem. B* **2003**, *107*, 12973−12980.
(64) Dalconi, M. C.; Alberti, A.; Cruciani, G.; Ciambelli, P.; Fonda, E. Siting and coordination of cobalt in ferrierite: XRD and EXAFS studies at different Co loadings. *Microporous Mesoporous Mater.* **2003**, *62*, 191−200.
(65) Kaucký, D.; Dědeček, J.; Wichterlová, B. Co^{2+} ion siting in pentasil-containing zeolites II. Co^{2+} ion sites and their occupation in ferrierite. A VIS diffuse reflectance spectroscopy study. *Microporous Mesoporous Mater.* **1999**, *31*, 75−87.

https://doi.org/10.1021/acs.jpcc.2c02496
J. Phys. Chem. C 2022, 126, 10686−10702